2011

STABILITY AND SPECTROSCOPIC PROPERTIES OF NEGATIVE IONS

Swayamprabha Behera
Virginia Commonwealth University

STABILITY AND SPECTROSCOPIC PROPERTIES OF NEGATIVE IONS

A thesis submitted in partial fulfillment of the requirements for the degree of Master of Science, at Virginia Commonwealth University.

by

Swayamprabha Behera

M.S. in Physics

Virginia Commonwealth University, 2010

Director: Dr. Purusottam Jena, Distinguished Professor, Department of Physics

Virginia Commonwealth University
Richmond, Virginia
May 2011

Acknowledgement

I am heartily thankful to my advisor, Dr. Purusottam Jena, whose encouragement, supervision and support from the preliminary to the concluding level enabled me to develop an understanding of the subject. In spite of his busy schedule, he gave me sufficient time to discuss with me on my research work. One simply could not wish for a better or friendlier advisor.

A special thank of mine goes to my research group members (Mary, Jorly, Devleena, Miao Miao, Kalpa) and all other classmates who helped me while studying in the department and motivated me.

I like to thank Dr. Alison Baski and all other Professors for their encouragement and moral support. Thanks to Dr. Dexian Ye and Dr. Hani El-Kaderi for their valuable advice and for being my defense committee member.

At last but not the least, I wish to thank my husband Govind as well as my parents and family members for their undivided support and inspiration without whom I would be unable to complete my degree.

Table of Contents

List of Tables

Table Page

List of Figure

Figure Page

Abstract

STABILITY AND SPECTROSCOPIC PROPERTIES OF NEGATIVE IONS

By Swayamprabha Behera, M.S.

A thesis submitted in partial fulfillment of the requirements for the degree of Master of Science, at Virginia Commonwealth University

Virginia Commonwealth University, 2011.

Major Director: Dr. Purusottam Jena, Distinguished Professor, Department of Physics

Negative ions play an important role in chemistry as building blocks of salts and oxidizing agents. Halogen atoms, due to their ability to attract electrons, readily form negative ions. Considerable interest exists in the design and synthesis of new negative ions called superhaogens whose electron affinities are much higher than those of halogen atoms. This thesis deals with the design of such species. Using density functional theory I have studied two classes of superhalogens. First one involves d^1 transition metal (Sc, Y, La) atoms surrounded by Cl while the second one involves simple metals (Na, Mg, Al) surrounded by pseudohalogens such as CN. Geometry, electronic structure, and electron affinity of these species containing up to 5 ligands have been calculated. Studies reveal a fundamental difference between the interaction of transition and metal atoms with electronegative ligands. In addition, pseudohalogens can be used to synthesize a new class of superhalogens.

Chapter 1: Introduction

1.1 Overview

There is considerable interest in studying negative ions not only because they are among the best known oxidizing agents [1] but also they play an important role in atmospheric chemistry by acting as nucleation centers [2]. Among the elements in the Periodic Table, halogen atoms are the most electronegative because they possess a hole in the outermost p-shell (ns^2np^5 electronic configuration), which can readily accommodate an electron in order to close the np shell. An extra electron attachment to a halogen atom results in the negatively charged ion whose total energy is significantly lower than that of the corresponding neutral. Consequently, the halogen atoms possess the highest electron affinities [3] (3.0–3.6 eV) among all the elements, with Cl having the largest value (~ 3.6 eV). However, the EA of a polyatomic system may exceed the 3.6 eV atomic limits due to collective effects.

In 1962, Bartlett synthesized the first chemically bound Xenon in $Xe^+ [PtF_6]^-$ [Ref:4]. He estimated the electron affinity of PtF_6 to be at least 6.76 eV [5]. This milestone work started the Chemistry of Nobel Gases, which previously have been considered as absolutely inert atoms. Since then, numerous molecules with high EAs were used to synthesize a wide variety of new chemical compounds, in which very strong oxidizers were required. Later Gutsev and Boldyrev

[6, 7], termed this class of molecules as superhalogens and gave the formula for such species, $MX_{(m+1)/k}$, where m is the nominal valence of the metal atom M and k is the valence of the electronegative ligand X. The resulting superhalogen anions have extremely high electron detachment energies due to the delocalization of the extra electron over the electronegative atoms. The EAs of many superhalogens have been estimated both theoretically [8, 9, 10, 11, 12] and experimentally [13, 14, 15]. First experiment to verify this assignment for superhalogens was carried out by Wang and coworkers [16].

Superhalogens are used in the synthesis of many new materials including organic metals and organic superconductors [17] many of which are highly energetic. Some superhalogen anions are commonly found as building blocks in condensed phase materials and gas phase molecules. The electron affinities of some of these superhalogens can be as high as 14 eV. Such large electron affinities suggest that these species can be used to extract electrons from the core orbital's of some atoms and form new compounds that otherwise do not exist.

1.2 Motivation and Current Work

Exploring various new superhalogen species is primarily focused on studying molecular clusters which are capable of forming strongly bound anions. The purpose of these efforts is to provide reliable data and predictions considering the possible use of such compounds as electron acceptors in the production of organic superconductors, as well as the role they can play in synthesis (e.g., in the oxidation of counterpart systems with high ionization potentials).

1.2.1 The onset of Super halogen Behavior of d^1 Transition metal chloride clusters

While considerable amount of work on superhalogen involving sp metals have been carried out [18, 19, 20, 21, 22, 23, 24] work on transition metal containing superhalogens are limited [25, 26].

A systematic study of the electron affinity of transition metals as a function of halogen content, however, can reveal interesting physics and chemistry. This is because the partially filled d-electrons can contribute to the valence of transition metals due to the small gap between d and s orbitals. For example, Manganese with an orbital configuration of $3d^5 4s^2$ is known to exhibit oxidation states ranging from -3 to + 7. Thus, it is a priori not clear for what composition of halogen atoms MX_n clusters will exhibit superhalogen behavior. In addition, how would this behavior change from 3d to 4d to 5d elements?

Recently photoelectron spectroscopy experiments have been carried out for MCl_4 (M = Sc, Y, La) and their vertical detachment energies have been measured [27, 28]. These are rather large, in the range of 7 eV, and clearly show that they behave as superhalogens. However, experiments containing lesser number of Cl atoms have not yet been performed, and so it is not clear how this superhalogen property evolves. To gain a detailed understanding of how each addition of chlorine to d^1 transition metal changes its electron affinity we carried out a systematic study of the equilibrium geometry, electronic structure, vertical detachment energies, and electron affinities of (MCl_n; M = Sc, Y, La; n = 1–5) clusters using density functional theory. The computational procedure and the results are discussed in Chapter 3.

1.2.2 Singly and doubly charged anions of chloride and pseudohalogen clusters:

Numerous investigations have been carried out on singly negative atomic and molecular ions both experimentally and theoretically. But the information on free doubly negative charged atomic and molecular charge is scarce. Multiply charged anions, on the other hand, mostly exist in solutions, on surfaces, or as building blocks of condensed matter systems where they are stabilized by charges on counter ions. Since the stability and electronic properties of multiply charged anions in the above systems are influenced by the medium they exist in, their fundamental understanding without the influence of the environment can only be achieved in the gas phase. The most important question concerns the critical size of a gas phase multiply charged anion. In these systems the Coulomb repulsion between the added charges has to be balanced by the binding energy of the constituent atoms that hold them together. An unstable multiply charged anion in the gas phase can either eject an electron or fragment into binary species to stabilize itself.

There have been several reports on doubly charged negative ions of fairly large organic molecules [29, 30, 31, 32]. For example, a long lived stable organic dianion is the dimer of benzo[*cd*] pyren-6-one, a large organic ketone. It was the first long-lived doubly charged negative ion to be observed in the gas phase [29]. Several theoretical [32, 33, 34] and experimental [35, 36] investigations have been carried out in search of small stable dianions. The smallest known long lived dianions thus far are found to be the alkali trihalide AX_3^{2-} (A= Li, Na, K and X=F or Cl) whose existence has been predicted theoretically by Scheller and Cederbaum

[33, 34] and experimentally verified [37]. The dianionic earth alkaline tetrahalides EX_4^{2-} (E= Be, Mg, Ca and X=F or Cl) have also been predicted in 1991 [37,38] theoretically and later verified experimentally [36].

We address both the issues of designing superhalogens with different electronegative ligands and using these concepts to study the critical size for the stability of their dianions in the gas phase. In the first part we use Cl as a ligand and present a systematic study of the structure, stability, and spectroscopic properties of neutral, single and doubly charged negative ions of MCl_n (M= Na, Mg, Al) clusters. In the second part, we replace the Cl ligand by psuedohalogen or halogenoid (–CN or –NC). The purpose of using the pseudohalogen is to understand how the geometry, electronic structure and the stability of the dianions change as the size of the ligand increases. The computational procedure and the results are discussed in Chapter 4.

Chapter 2: Theoretical Method

All calculations have been carried out using density functional theory (DFT) with B3LYP hybrid functional for exchange and correlation (XC) potential. The accuracy of the DFT-based results is verified by carrying selected calculations using other *ab initio* quantum-chemical methods such as MP2 (second order Moller-Plesset Perturbation), CCSD(T) (Coupled Cluster with single and double excitations).

2.1 Introduction

The quest for a practical theory to calculate the electronic properties of an N-electrons system is almost a century old. A theoretical path towards this goal was first proposed by Schrödinger in 1927, using the concept of wave mechanics as a tool.

According to Schrodinger, the electronic properties of much particle system can be determined from its wave function Ψ, the solution of the time-independent Schrödinger equation:

$$\hat{H}\,\Psi = E\,\Psi \qquad (2.1)$$

where $\hat{H}$ is Hamiltonian operator and E is an Eigen value.

Hamiltonian operator $\hat{H}$ is a differential operator that acts on the total wave function and can be written as [39]

$$H = -\frac{\hbar^2}{2m_e}\sum_{i=1}^{N}\nabla_i^2 - \frac{\hbar^2}{2M_A}\sum_{A=1}^{M}\nabla_A^2 - e^2\sum_{i=1}^{N}\sum_{A=1}^{M}\frac{Z_A}{r_{iA}} + e^2\sum_{i=1}^{N}\sum_{j>i}^{N}\frac{1}{r_{ij}} + e^2\sum_{A=1}^{M}\sum_{B>A}^{M}\frac{Z_A Z_B}{r_{AB}} \qquad (2.2)$$

where i and j run over N electrons and A, B run over M nuclei. Z_A and Z_B are atomic number, M_A and m_e are the mass of nucleus and electron respectively, $\hbar = \frac{h}{2\pi}$ where h is the Planck's constant. The first two terms are kinetic energy (T) of electron and nuclei respectively. The third term (potential energy term) is attractive electrostatic interaction between the nuclei and electrons (V_{Ne}). The fourth and fifth terms are potential energy due to electron–electron (V_{ee}) and nucleus–nucleus interaction respectively. Both terms are repulsive in nature. Here the Laplacian operator ∇_q^2 is defined as sum of differential operators.

$$\nabla_q^2 = \frac{\partial^2}{\partial x_q^2} + \frac{\partial^2}{\partial y_q^2} + \frac{\partial^2}{\partial z_q^2} \qquad (2.3)$$

The exact solution Ψ for the equation (2.1), however has been a challenge to many, for most of the last century. The electronic structure studies of large clusters and solid having interesting phenomena, like chemisorptions study are computationally very expensive and hence demand simplified schemes.

The major step toward simplifying the above problem is by the application of Born–Oppenheimer approximation [40]. This approximation is valid, only when the ratio of electron to nuclear mass is considerable small. Therefore, the kinetic energy of the nucleus is assumed to be zero and repulsive potential energy due to nucleus–nucleus interactions can be assumed to be

almost constant. Thus, the complete Hamiltonian is given by equation (2.2) reduces to so called electronic Hamiltonian H_{ele} is given by :

$$H_{ele} = -\frac{\hbar^2}{2m_e}\sum_{i=1}^{N}\nabla_i^2 - e^2\sum_{i=1}^{N}\sum_{A=1}^{M}\frac{Z_A}{r_{iA}} + e^2\sum_{i=1}^{N}\sum_{j>i}^{N}\frac{1}{r_{ij}} = T + V_{Ne} + V_{ee} \qquad (2.4)$$

The attractive potential V_{Ne} is often termed as external potential V_{ext} in density functional theory. Now, the main task of the electronic structure calculation is reduced to solving the electronic Schrödinger equation.

However, it can be exactly solved only for a single electron system. Approximations are required to solve multi-electron systems because of the complexity of electron–electron interaction in much particle system.

2.2 – Hartree approximation

In this approximation [41], the one–N electron problem is separated into N–one electron Schrödinger equations. Here the Hamiltonian has the form:

$$H = \sum_{i=1}^{N} h(i) \qquad (2.5)$$

where *h(i)* is the operator describing kinetic energy and potential energy of electron i and is defined as

$$h(i) = -\frac{1}{2}\nabla_i^2 - \sum_{A=1}^{M}\frac{Z_A}{r_{iA}} + e^2\sum_{j=1}^{N}\frac{1}{r_{ij}} \qquad (2.6)$$

The wave function is a simple product of spin orbital wave functions for each electron and is defined as Hartree product wave function.

The Hartree product [42] wave function is given by:

$$\Psi^{HP}(x_1, x_2, ...x_n) = \chi_i(x_1)\chi_j(x_2)....\chi_k(x_N) \quad (2.7)$$

where χ_i is spin orbital *i* (solution of one particle Schrodinger equation), x_i is position and spin of electron *i*. The function uses Hartree equation. The Hartree equation is an eigenvalue equation of the form:

$$h(i)\chi_j(x_i) = \varepsilon_j \chi_j(x_i) \quad (2.8)$$

Schrödinger equation for whole system is of the form:

$$H\psi^{HP} = E\psi^{HP} \quad (2.9)$$

Here eigenvalue, E is sum of spin orbital energies of each spin orbitals appearing in ψ^{HP}

$$E = \varepsilon_i + \varepsilon_j + ... + \varepsilon_k \quad (2.10)$$

The Hartree method provides a great foundation for numerically approximating many body systems. However, it has some drawbacks. The important one is that the total wave function is not anti-symmetric under interchange of electron coordinates and doesn't obey the Pauli Exclusion Principle.

2.3 – Hartree- Fock approximation

In Hartree –Fock [42,43] approximation, the total wave function of the N-electron system is approximated by an anti-summarized product of N one-electron wave functions $\chi_i(x_i)$. This

product is usually represented by a determinant called *Slater determinant* ψ_{SD} [44]. Here the correlated electron-electron repulsion is not specifically taken into account, only its average effect is included in the calculation.

$$\psi_{SD}(x_1, x_2, \ldots x_N) = \frac{1}{\sqrt{N!}} \begin{pmatrix} \chi_1(x_1) & \chi_2(x_1) & \ldots & \chi_N(x_1) \\ \chi_1(x_2) & \chi_2(x_2) & \ldots & \chi_N(x_2) \\ . & . & \ldots & . \\ . & . & \ldots & . \\ . & . & \ldots & . \\ \chi_1(x_N) & \chi_2(x_N) & \ldots & \chi_N(x_N) \end{pmatrix} \qquad (2.11)$$

Where $\frac{1}{\sqrt{N!}}$ is the normalization factor. $\chi_i(x_i)$ is called spin orbital of particle *i*.

In the Hartree-Fock (HF) approximation, the antisymmetry property of electrons is accounted. $\Psi(x_1, x_2)$ is antisymmetric with respect to the interchange coordinates of electron one and two.

$$\Psi(x_1, x_2) = - \Psi(x_2, x_1) \qquad (2.12)$$

The Slater determinant obeys Pauli Exclusion Principle. When two electrons are assigned to the same spin orbital, i.e. χ_1 and χ_2 is same, then the determinant will be zero.

The Hartree-Fock equation is an eigenvalue equation of the form:

$$f(i)\chi_j(x_i) = \varepsilon_i \chi_j(x_i) \qquad (i = 1, \ldots N) \qquad (2.13)$$

where ε_i is eigen solutions of N number of equations, χ_j is spin orbital *j* and *f(i)* is an effective one-electron operator, called the *Fock* operator, of the form:

$$f(i) = -\frac{1}{2}\nabla_i^2 - \sum_{A=1}^{M} \frac{Z_A}{r_{iA}} + v^{HF}(i) \qquad (2.14)$$

where $v^{HF}(i)$ is *Hartree-Fock potential* (average repulsive potential experienced *ith* electron due to remaining N-1 electrons). Thus, the complicated two-electron repulsion operator $1/r_{ij}$ in the Hamiltonian is replaced by the simple one-electron operator $v^{HF}(i)$ where the electron-electron repulsion is taken into account only in an average way. $v^{HF}(i)$ has following two components:

$$v^{HF}(i) = \sum_{j}^{N} J_i(x_i) - K_j(x_i) \qquad (2.15)$$

where *J* and *K* are Coulomb and exchange operators, respectively.

The total energy for the HF approximation is given as below:

$$E_{HF} = \langle \psi_{SD} | H | \psi_{SD} \rangle = \sum_{i=1}^{N} \varepsilon_i - \frac{1}{2} \sum_{i=1}^{N} \sum_{j=1}^{N} (J_{ij} - K_{ij}) = \sum_{i=1}^{N} \varepsilon_i - \langle \psi_{SD} | V_{ee} | \psi_{SD} \rangle \qquad (2.16)$$

where the Coulomb integral (due to pair-wise Coulomb interaction between the i^{th} electron and the other electrons in all occupied spin orbitals) is given by:

$$J_{ij} = \langle ii | jj \rangle = \int dx_i dx_j \frac{|\chi_i(x_i)|^2 |\chi_j(x_j)|^2}{r_{ij}} \qquad (2.17)$$

and exchange integral, exchange of two variables within spin orbitals, is given by:

$$K_{ij} = \langle ij | ji \rangle = \int dx_i dx_j \frac{\chi_i^*(x_i)\chi_j(x_i)\chi_j^*(x_j)\chi_i(x_j)}{r_{ij}} \qquad (2.18)$$

However, due to the Coulomb and Exchange terms appearing in the Hartree-Fock (HF) Hamiltonian, solving the Schrödinger equation involves calculating large number of two-electron intergrals. Hence the HF method requires greater computational effort, compared to that for

Hartree method. Moreover, the HF approximation doesn't take into account the short-range (*dynamical*) correlation between the electrons. This is due to the fact that the wave function ψ is represented as a rigid single *Slater determinant* which makes the electrons interact with the average potential due to other electrons, instead of pair wise interactions. Hence, this method fails in describing the bond strengths, giving energies with an error of about 1 percent.

In order to include the *dynamical correlation*, the many-body wave function is represented by a linear combination of *Slater determinants*. The Configuration Interaction (CI) method or multi-configuration expansion includes these multi-determinantal wave functions. Many types of calculations begin with a Hartree–Fock calculation and subsequently correct for electron-electron repulsion, referred to also as electronic correlation. Møller–Plesset perturbation theory (MP_n) and coupled cluster theory (CC) are examples of these post-Hartree–Fock methods. However, due to these required large number of the configurations, it become computationally expensive to employ this Post Hartree-Fock method for large systems. Hence the application of these methods is usually limited to relatively smaller molecules/clusters, where an accurate representation of the electron system is possible.

Several promising approximations have been developed to incorporate the energy and also to balance the computational time/cost with accuracy of the results. Thomas and Fermi, proposed a different method, in which, instead of the wave function ψ, the total electron charge density ρ was considered. The electron charge density of an N particle system is given by:

$$\rho(r) = N \int dx_1 \ldots \int dx_N \, \psi^* (x_1, \ldots x_n) \, \psi(x_1, \ldots x_n) \qquad (2.19)$$

This theory can be seen as the starting points towards the development of *Density Functional Theory* (DFT).

2.4 Density Functional Theory (DFT)

DFT is a quantum mechanical method used in physics and chemistry to investigate the electronic structure of many-body systems and is based on the fact that electron density can be used to describe the fundamental properties of an N-electron system. In 1964, Hohenberg and Kohn [45] proved that the ground state energy of an N-electron system can be represented as functionals of electron density, ρ that depends only on three spatial coordinates. It lays the groundwork for reducing many-body problem of N electrons with 3N spatial coordinates to 3 spatial coordinates, through the use of functional of electron density.

2.4.1 Hohenberg-Kohn Formulation

Under the Born-Oppenheimer approximation, the Hamiltonian of an N-electron system can be represented as:

$$H = \sum_{i=1}^{N}(-\frac{\nabla_i^2}{2}) + \sum_{i=1}^{N} V(\vec{r}_i) + \frac{1}{2}\sum_{i\neq j}^{N}\frac{1}{r_{ij}} \qquad (2.20)$$

Where $V(\vec{r}_i)$ known as external potential, is the potential created by the nuclei over electron *i*, and is given by:

$$V(\vec{r}_i) = -\sum_{A=1}^{M}\frac{Z_A}{r_{iA}} \qquad (2.21)$$

The ground state electronic energy for this system can be determined by the minimization of the functional $E[\Psi]$, using the variational principle

$$E[\psi] = \frac{\langle \psi | H | \psi \rangle}{\langle \psi | \psi \rangle} \qquad (2.22)$$

Hence, for an N-electron system, the external potential $V(\vec{r})$ completely fixes the Hamiltonian; Thus N and $V(\vec{r})$ determine all the ground state properties. According to Hohenberg-Kohn theorems, the ground state electron density ρ, instead of N, $V(\vec{r})$, determines the properties of the system, hence every observable can be represented as a functional of $\rho(\vec{r})$.

The Density Functional Theory is based on two famous lemma due to Hohenberg and Kohn. *The first lemma states that: The external potential* $V(\vec{r})$*, can be determines within a trivial additive constant, by the electron density* $\rho(\vec{r})$. A simple proof of this theorem is based on the minimum energy principle for the ground state, was provided by Hohenberg and Kohn in their work. The total energy, therefore, can be represented in terms of the electron density ρ as:

$$E[\rho] = T[\rho] + V_{ne}[\rho] + V_{ee}[\rho] \qquad (2.23)$$

where T[ρ] is the kinetic energy, $V_{Ne}[\rho]$ is the potential energy due to the electron-nuclei interaction, and the third term $V_{ee}[\rho]$, represents the potential energy due to the electron-electron interactions. The above equation can be rewritten as:

$$E[\rho] = \int \rho(\vec{r}) V(\vec{r}) d\vec{r} + F_{HK}[\rho] \qquad (2.24)$$

where $F_{HK}[\rho] = T[\rho] + V_{ee}[\rho]$ (2.25)

where the $V_{ee}[\rho]$ can be written as sum of two parts: J[ρ], the Coulomb electrostatic interaction between electron and $E_{non\text{-}classical}[\rho]$, the non-classical part, called Exchange-Correlation energy. It is to be noted here that the F_{HK} doesn't depend on the external potential V, and hence is a university functional and is identical for every system.

The second lemma of Hohenberg-Kohn deals with the variational principle. It states: For any trial density $\tilde{\rho}(\vec{r})$, *such that* $\tilde{\rho}(\vec{r})d\vec{r} \geq 0$ *and* $\int \tilde{\rho}(\vec{r})d(\vec{r}) = N$,

$$E_{ground} \leq E[\rho(r)] \qquad (2.26)$$

Hence, the energy of the system is represented and minimized with respect to the electron density ρ. As the functional F_{HK} is a universal functional, if we can construct as approximate form of the functional, it can be applied to any real system. The earliest approximation for this functional was provided by Thomas [1927], Fermi [1928] and Dirac [1930], even before the advent of Hohenberg-Kohn theorems. Kohn and Sham in 1965, modified this equation by introducing the orbital and by a clever mixing of the interacting and non-interacting terms and paved the way for practical application of DFT.

2.4.2 Kohn-Sham Equations

In Kohn-Sham [46] density functional theory, one imagines that a system of independent non-interacting electrons moving in a common, one body potential V_{eff} (one electron potential) yields the same density as the "real" fully-interacting system. A set of independent orbitals Φ_i (Kohn-Sham orbitals) satisfy the following independent single particle Schrödinger equation:

$$(-\frac{1}{2}\nabla^2 + V_{eff}(\vec{r}))\varphi_i(\vec{r}_i) = \varepsilon_i\varphi_i(\vec{r}) \qquad (2.27)$$

where the first term is the kinetic energy of the non-interacting electrons defined as ($T_S[\rho]$). The local one-body potential V_{eff} (one electron potential) is derived from the non-interacting density:

$$\rho(\vec{r}) = \sum_{i=1}^{N} |\varphi_i(\vec{r})|^2 \qquad (2.28)$$

The above single-particle Schrödinger equations are valid for systems with interacting particles, which satisfy:

$$V_s(\vec{r}) \equiv V_{eff}(\vec{r}) = V_C + V_{XC}(\vec{r}_1) - V_{Ne} = \int \frac{\rho(\vec{r}_2)}{r_{12}} d\vec{r}_2 + V_{XC}(\vec{r}_1) - \sum_{A=1}^{M} \frac{Z_A}{r_{1A}} \qquad (2.29)$$

where V_C is the classical Coulomb potential, V_{xc} is exchange-correlation potential and V_{Ne} or V_{ext} is external energy due to nuclei-electron interaction. V_{xc} is simply defined as the functional derivative of E_{xc} with respect to ρ, i.e.,

$$V_{XC} = \frac{\delta E_{XC}[\rho]}{\delta\rho(\vec{r})} \qquad (2.30)$$

Then we express the total electronic energy of the real, fully interacting system as,

$$E[\rho(\vec{r})] = T_s[\rho] + J[\rho] + E_{xc}[\rho] + E_{Ne}[\rho]$$
$$= -\frac{1}{2}\sum_{i=1}^{N}\langle\varphi_i|\nabla^2|\varphi_i\rangle + \frac{1}{2}\sum_{I=1}^{N}\sum_{j=1}^{N}\iint|\varphi_i(\vec{r}_1)^2|\frac{1}{r_{12}}|\varphi_j(\vec{r}_2)|^2 d\vec{r}_1 d\vec{r}_2 + E_{xc}[\rho(\vec{r})] - \sum_{i}^{N}\int\sum_{A=1}^{M}\frac{Z_A}{r_{1A}}|\varphi_i(\vec{r}_1)|^2 d\vec{r}_1 \qquad (2.31)$$

where the first term is the kinetic energy of a non-interacting system ($T_S[\rho]$), the second

term is the classical electrostatic electron-electron repulsion energy ($J[\rho]$), the third term is exchange-correlation energy of particle $E_{xc}[\rho]$, and the last term is energy due to nuclei-electron interaction ($E_{Ne}[\rho]$). The kinetic energy is represented in terms of corresponding orbital instead of electron density ρ.

2.4.3 Exchange-Correlation Functional

The exact form of exchange-correlation energy (E_{xc}) is difficult to obtain. Hence, in DFT, one uses an approximate form for E_{xc}, which may give accurate results. V_{xc} depends on the electron density at every point. E_{xc} can be treated in two parts:

$$E_{xc}[\rho(\vec{r})] = E_x[\rho] + E_c[\rho] = \int \rho(\vec{r})\varepsilon_x d\vec{r} + \int \rho(\vec{r})\varepsilon_c d\vec{r} \qquad (2.32)$$

where E_x is the exchange energy of the Slater determinant of Kohn-Sham orbital in equation (2.27). E_c is the correlation energy, ε_x is exchange energy per particle and ε_c is correlation energy per particle. In general, the contribution of exchange energy, E_x is larger than the correlation energy E_c .

2.4.3.1 Local Density Approximation (LDA)

This is the first approximation made to E_{xc}. It is based on the homogenous electron gas. In this approximation, the electron density is assumed to be a slowly varying function of $\vec{r}$. The exchange energy, E_x in LDA approximation is defined as:

$$E_x^{LDA} = -\frac{3}{4}\left(\frac{3}{\pi}\right)^{1/3} \int \rho(\vec{r})^{4/3} d\vec{r} \qquad (2.33)$$

where exchange energy per particle is,

$$\varepsilon_x^{LDA}[\rho] = -\frac{3}{4}(\frac{3}{\pi})^{1/3}\rho(\vec{r})^{1/3} \qquad (2.44)$$

Therefore, the corresponding local exchange potential is given as:

$$V_x^{LDA}(\rho) = \frac{\partial E_x^{LDA}}{\partial \rho} = -(\frac{3}{\pi})^{1/3}\rho(\vec{r})^{1/3} \qquad (2.45)$$

The most widely used LDA functional is the VWN (Vosko, Wilk and Nusair) [47] correlation functional which is given in the form of:

$$\varepsilon_c^{VWN} = \frac{A}{2}[\ln\frac{x^2}{X(x)} + \frac{2b}{Q}\tan^{-1}\frac{Q}{2x-b} - \frac{bx_0}{X(x_0)}(\ln\frac{(x-x_0)^2}{X(x)} + \frac{2(b+2x_0)}{Q}\tan^{-1}\frac{Q}{2x-b})] \qquad (2.46)$$

where $x = r_s^{1/2}$ (r_s: effective volume containing one electron), $X(x) = x^2 + bx + c$, and $Q = (4c-b^2)^{1/2}$ and A, x_0 and c are constants.

The LDA exchange-correlation energies are insufficiently negative (by about 10%) for almost all atoms. The LDA is a reliable, moderate-accuracy approximation. However, LDA is not accurate enough for most chemical applications, which require the determination of energy differences with considerable accuracy. It overestimates bonding and in turn underestimates equilibrium volume; underestimate bond gap; gives too large bulk modulus.

2.4.3.2 Generalized Gradient Approximation (GGA)

Several attempts have been made to improve the LDA, and one of the most important is the inclusion of gradient corrections in the E_{xc}. Here the functional are dependent on both the density ρ and its gradient, $\nabla\rho$. Gradient-corrected functional is of the following form:

$$E_c^{GGA}[\rho] = \int \rho(\vec{r})\varepsilon_{xc}[\rho(\vec{r}), \nabla(\vec{r})]d\vec{r} \qquad (2.47)$$

Becke proposed a correction to the LDA exchange energy that has the correct asymptotic behavior (1/r) (in the LDA exchange the density has an exponential dependence on r in the asymptotic region). The gradient corrected exchange functional due to Becke (B88) [48, 49] is given as:

$$E_x^{B88} = E_x^{LDA} + \Delta E_x^{B88} \qquad (2.48)$$

Where $\Delta E_x^{B88} = -\beta\rho^{1/3}\frac{x^2}{1+6\beta x \sinh^{-1} x}$ (2.49)

where β is a parameter determined from atomic data, and $x = \frac{|\nabla\rho|}{\rho^{4/3}}$

2.5 B3LYP Hybrid Density Functional

In 1993, Becke [48,49] gave a gradient corrected exchange functional, which is a combination of both the exact HF exchange and DFT exchange energies, hence termed hybrid functional. In the B3LYP hybrid functional scheme, the non local HF is mixed with the energy functional of Generalized Gradient Approximation (GGA). Here, the Perdew-Wang [50] gradient-corrected correlation energy, which was used in the original work of Becke, is replaced with the Lee-Yang-Parr correlation energy [51]. It is a combination of the Slater40 [LDA exchange], HF and Becke's gradient correction for exchange and with Lee, Yang and Parr gradient corrected correlation functional. The B3LYP has the form:

$$E_{xc}^{B3LYP} = E_x^{LDA} + a_0(E_x^{HF} - E_x^{LDA}) + a_x\Delta E_x^{B88} + E_c^{VWN} + a_c(E_c^{LYP} - E_c^{VWN}) \qquad (2.50)$$

where a_0 = 0.20, a_x =0.72 and a_c =0.81 are semi-empirical coefficients, determined by

fitting to experimental data. Here the LDA of Vosko, Wilk, and Nusair[47] is used for E_x^{LDA} and E_c^{VWN}. E_x^{HF} is the exact non-local HF exchange energy. E_x^{B88} and E_x^{LYP} are the Becke's and Lee-Yang-Parr's gradient corrections for the local exchange and correlation energies, respectively.

2.6 Basis Sets

The molecular orbitals Ψ_i are represented as linear combination of a finite set of predefined N- one electron functionals, known as basis functions, χ_μ.

$$\psi_i = \sum_{\mu=1}^{N} C_{\mu i}\chi_\mu \qquad (2.51)$$

where $C_{\mu i}$ are molecular orbital expansion coefficients, χ_μ is the μ-th orbital and N is number of atomic orbitals. Often basis functions are atomic orbitals in Linear Combination of Atomic Orbitals.

There are two types of basis functions commonly used in the electronic structure calculations. They are *Slater Type Orbitals (STOs)*[52] and *Gausssian Type Orbitals (GTOs)* [53]. The Slater Type Orbitals are given as:

$$\chi(r,\theta,\varphi) = Nr^{n-1}e^{-\zeta r}Y_{l,m}(\theta,\varphi) \qquad (2.52)$$

where N is normalization constant, ζ is called "Slater orbital exponent". (r,θ,φ) are spherical coordinates, and $Y_{l,,m}$ are the conventional spherical harmonics. These functions are accurate as they reflect exponential decay of the wave function. However solving the three- and four-centered integrals with STOs are extremely expensive in SCF calculations.

To circumvent this problem GTOs basis functions come into picture. In cartesian coordinates GTOs can be written as:

$$\chi(x,y,z) = Nx^{l_x} y^{l_y} z^{l_z} e^{-\zeta r^2} \qquad (2.53)$$

where l_x , l_y and l_z determines the angular part of orbital and ζ represents the radial part of the function.

The use of *Gaussian-Type orbitals (GTOs)* reduces the computational cost but has some drawbacks. The e^{-r2} dependence, results in a zero slope at the nucleus.

Contracted basis sets were used to reduce computational expense of large number of basis functions describing each of the atomic orbitals. *The Contracted basis functions*, have fixed contraction and coefficients. χ_μ^{CGF} can be written as:

$$\chi_\mu^{CGF} = \sum_{i=1}^{L} d_{i\mu} \chi_i^{GF}(\varsigma_{i\mu}, r) \qquad (2.54)$$

where $d_{i\mu}$ is a contraction coefficient, L is the length of the contraction, and $\varsigma_{i\mu}$ is a contraction exponent.

Now, equation (2.51) can be rewritten as:

$$\psi_i = \sum_{\mu=1}^{N} C_{\mu i} \chi_\mu^{CGF} \qquad (2.55)$$

The widely used minimal basis set can be represented as STO-nG basis. In this basis set, each STO is given by contraction of n primitive GTOs. For example, 6-311G acronym implies that the valence basis functions are contractions of three primitive Gaussians (the inner function) and

one, one primitive Gaussians (the outer functions), whereas the inner shell functions (core orbital) are contraction of six primitive Gaussians. Polarization functions and diffuse functions are added to improve the basis set. Polarization functions (represented as *) enhance the 'flexibility" of atoms to form chemical bonds whereas diffuse functions (represented as +) improve the predicted properties of species with extended electron density such as anion. For example 6-31G** denotes that d-type functions is added to heavy atoms (left *), and p-type functions is added to hydrogen (right *). Similarly, in 6-31++G; diffuse functions are added to hydrogen (right +) and heavy atoms (left +).

Chapter 3

Computational Procedure, Results and discussion Of d^1 transition metal chloride clusters

3.1 Validation of Computational Procedure

We carried out all the computations using density functional theory (DFT) with generalized gradient approximation (GGA) as well as hybrid functional for exchange and correlation (XC) potential. We have used BPW91[54-56] for the hybrid functional. Similarly we have used 6-311+G(d) and 6-311+G(3df) basis sets for Cl and Sc and SDD basis set for Y and La. Calculations were carried out using the GAUSSIAN 03 package[57]. In Table 1 we compare the calculated ionization potentials and electron affinities of Sc, Y, La and Cl atoms for different basis sets and exchange correlation functionals.

Table 1: Comparison of calculated IP (Ionization Potential) and EA (Electron Affinity) of Sc, Y, La and Cl with experimental data [58]:

Elements	Sc	Y	La	Cl			
Properties	**IP (eV)**	**IP (eV)**	**IP (eV)**	**IP (eV)**	**EA (eV)**	**Bond Energy (eV)**	**Bond Length (Å)**
Experimental	6.54	6.38	5.58	12.97	3.62	2.49	1.98
BPW91/SDD	6.31	6.17	5.35	12.96	2.82	1.81	2.24
B3LYP/SDD	6.65	6.33	5.69	13.02	2.79	1.51	2.23
BPW91/6-311+G(d)	6.16	-	-	12.98	3.67	2.35	2.06
B3LYP/6-311+G(d)	6.56	-	-	13.07	3.72	2.06	2.05
BPW91/6-311+G(3df)	6.16	-	-	12.98	3.63	2.69	2.01
B3LYP/6-311+G(3df)	6.56	-	-	13.07	3.68	2.39	2.01

By comparing these with experimental results [59] we chose to use the B3LYP functional for the remaining calculations. For each cluster, MCl_n (M = Sc, Y, La; n = 2–5) several initial geometries were used with chlorine bound both molecularly (Cl_2) and atomically (Cl). Optimizations were carried out without any symmetry constraint. All the optimizations are followed by frequency calculations to confirm that the structures represent genuine minima in the potential energy surface. We have calculated the total energies as a function of spin multiplicities to obtain the preferred spin configurations of the neutral and anionic species. Thus, complete conformational search has been done at SDD/6-311+G(d) basis set level and the lowest energy isomers were re-optimized at SDD/6-311+G(3df) level. The vertical detachment energy,

VDE (the energy difference between the anion and its neutral at the anionic geometry) and electron affinity, EA (the energy difference between the ground states of the anion and its corresponding neutral) were calculated so that these can be compared with available experimental data involving photoelectron spectroscopy.

3.2 Results

Here we have discussed the geometries, electronic structure, and electron affinities of MCl_n (M = Sc, Y, La; n = 1–5) separately.

3.2.1 MCl (M= Sc, Y, La)

In Figure 1 we provide the geometries of ScCl, YCl, and LaCl molecules. The bond lengths and charges obtained from the natural bond orbital (NBO) analysis are listed for the neutral. In the parentheses corresponding results are given for the anions.

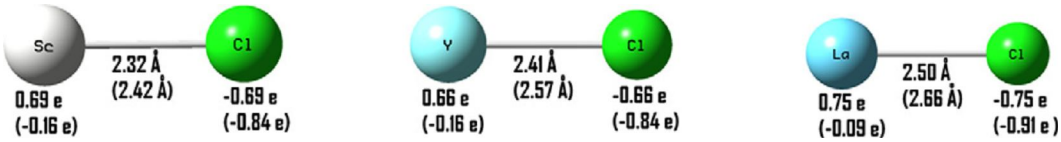

Figure:1. Structures of MCl (M = Sc, Y, La) at B3LYP/SDD/6-311+G(3df).

As seen from the above figure, the bond lengths for both the neutrals and anions increase from Sc to La as can be expected from the size of the Sc, Y and La atoms. The charge transfer from the metal atoms to Cl in the neutral molecule is about the same for all the three metals and

indicates that the bonding is dominated by ionic interaction. In the anions, the extra electron goes to neutralize the positive charge on the metal atoms and consequently the bond lengths are larger than those in the neutrals.

To obtain the preferred spin multiplicity of the ScCl, YCl and LaCl we calculated the total energies of the lowest two spin states, namely singlet and triplet for the neutrals and doublet and quartet for the anions. Spin triplet state of neutral ScCl is 0.24 eV lower in energy than the singlet state. The ground state spin multiplicity of YCl is a singlet which lies lower in energy than the triplet by 0.57 eV. For neutral LaCl, on the other hand, both singlet and triplet states are energetically nearly degenerate with the triplet only 2 eV higher in energy than the singlet. The degeneracy in the preferred spin is lifted in the anions. The preferred spin states for the $ScCl^-$, YCl^- and $LaCl^-$ are all doublets which lie 0.95, 0.94 and 1.13 eV, respectively, lower in energy than from the spin quartet states.

The computed electron affinities (EAs) and vertical detachment energies (VDEs) for two different basis sets are given in Table 2. We note that improving the basis sets only has marginal effect on the VDE and EA which are uniformly small in all cases. No experimental data are available to compare with our calculated results.

Table 2: EA of MCl and VDE of MCl^- (M = Sc, Y, La).

Method/Basis set	ScCl		YCl		LaCl	
	EA (eV)	VDE (eV)	EA (eV)	VDE (eV)	EA (eV)	VDE (eV)
B3LYP/SDD/6-311+G(d)	1.19	1.24	0.73	0.86	0.86	0.92
B3LYP/SDD/6-311+G(3df)	1.16	1.20	0.68	0.80	0.85	0.91

3.2.2 MCl_2 (M= Sc, Y, La)

The equilibrium geometries of all neutral and anionic MCl_2 clusters (M = Sc, Y, La) are given in Fig. 2 below along with their respective bond lengths and NBO charges.

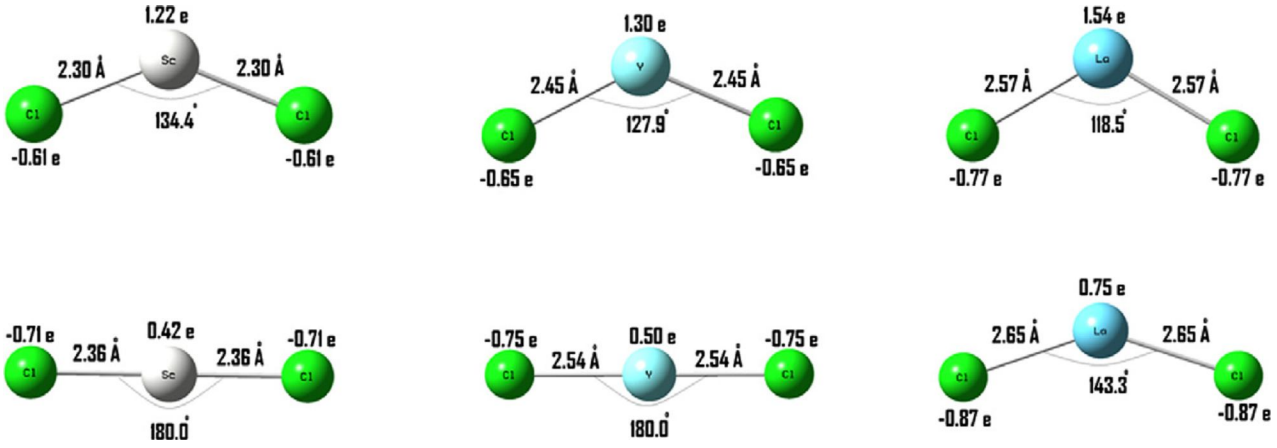

Figure 2. Structures of MCl_2 (top row) and MCl_2^- (bottom row) (M = Sc, Y, La) at B3LYP/SDD/6-311 + G(3df).

Note that all neutral clusters are bent structures while the $ScCl_2^-$ and YCl_2^- have linear structures. The geometry of $LaCl_2^-$, however, is a bent structure although the Cl–La–Cl bond angle in the anion is larger than that of the neutral. The bond lengths are similar to those in MCl and the anion bonds are larger than their corresponding neutrals. In neutral MCl_2 cluster, charge is transferred from the metal atoms to Cl, thus making the bonding predominantly ionic. When the extra electron is added to the anion, it preferentially goes to neutralize the positive charge on the metal atoms. The preferred spin states for neutral $ScCl_2$, YCl_2, and $LaCl_2$ clusters are doublet with the quartet states lying, respectively, 4.19, 4.59 and 4.50 eV higher in energy. This drastic rise in energy from doublets to quartets is due to the non-availability of electrons in valence orbitals that can be unpaired after the preferred two-center two-electron (2c–2e) bonds are formed. For the anions, however, the additional electron available for bonding reduces the energy difference between singlets and triplets; the triplets are only 0.08, 0.64, 0.36 eV higher than the singlets in $ScCl_2^-$, YCl_2^-, and $LaCl_2^-$, respectively.

The EA and VDE values are given in Table 3. We note that these values are again small, although they are slightly larger than those of their MCl (see Table 2) counterparts. Again, no experimental data are available to compare with our calculated results.

Table 3: EA of MCl_2 and VDE of MCl_2^- (M = Sc, Y, La).

Method/Basis set	$ScCl_2$		YCl_2		$LaCl_2$	
	EA (eV)	VDE (eV)	EA (eV)	VDE (eV)	EA (eV)	VDE (eV)
B3LYP/SDD/6-311+G(d)	1.50	1.61	1.68	1.84	1.27	1.40
B3LYP/SDD/6-311+G(3df)	1.41	1.52	1.58	1.73	1.24	1.36

3.2.3 MCl_3 (M= Sc, Y, La)

The equilibrium geometries of neutral $ScCl_3$, YCl_3, and $LaCl_3$ are given in Fig. 3. The geometries of their anions are similar to those of their neutrals, which is trigonal planar. Thus, in Fig. 3 we have given the bond lengths and NBO charges of the anions in parentheses. The bond lengths between metal atoms and Cl are similar to those seen in Figs. 1 and 2. The ground state spin configurations of the neutral clusters are all singlets while those for the anions are doublets. The spin triplet states of the neutrals are 3.68, 3.98 and 4.28 eV, respectively, higher in energy than the singlets in $ScCl_3$, YCl_3, and $LaCl_3$. Correspondingly, the quartet states of the anions are 4.77, 4.98 and 4.92 eV higher in energy than the spin doublet states.

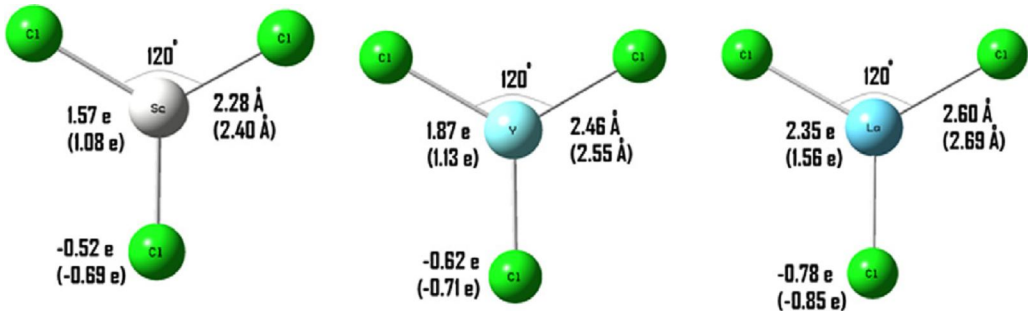

Figure3. Structures of MCl_3 (M = Sc, Y, La) at B3LYP/SDD/6-311 + G(3df).

We note that in neutral MCl_3 clusters, charge is transferred from the metal atom, M to Cl and this charge transfer increases from Sc to La. This is consistent with the decreasing ionization potential as one proceeds from Sc to La (see Table 1). In the anions, significant portion of the extra electron goes to the metal site.

MCl_3 is the most stable species as it consumes all its valence electrons when interacting with three Cl atoms and all the three bonds are classic two-center two-electron bonds. It should be kept in mind that in solids with composition MCl_3, metals have higher coordination; 6 for $ScCl_3$ [60] and YCl_3 [61] and 9 for $LaCl_3$ [62]. The high ionic nature of the bonding is apparent from the high charge for Cl in gas phase calculation and also negligible change in atomic charge of Cl in MCl_n series. The VDE and EA values of $ScCl_3$, YCl_3, and $LaCl_3$ are given in Table 4. These values only show a marginal increase over those in Tables 2 and 3. Once again, no experimental results are available to compare with our calculated results

Table 4: EA of MCl_3 and VDE of MCl_3^- (M = Sc, Y, La).

Method/Basis set	$ScCl_3$		YCl_3		$LaCl_3$	
	EA (eV)	VDE (eV)	EA (eV)	VDE (eV)	EA (eV)	VDE (eV)
B3LYP/SDD/6-311+G(d)	2.15	2.43	1.94	2.08	1.56	1.70
B3LYP/SDD/6-311+G(3df)	2.01	2.28	1.77	1.90	1.53	1.66

3.2.4 MCl_4 (M= Sc, Y, La)

MCl_4 represents the first neutral cluster having electron deficient bonding. This is reflected in the geometry of the neutral clusters which are shown in Fig. 4.

Here the electron deficiency resulted in multicenter bonding with one Cl–M–Cl bond angle being around 60º while the other bond angles are around 120º. The clusters have C_{2v} symmetry. The bond lengths between the metal atom and Cl are relatively unchanged from those described earlier for the bonds involving electron sufficient bonding, but the electron deficient bonds are lengthened. Similarly the atomic charges on chlorines involved in electron deficient bond are remarkably less. When an extra electron is attached, the geometries of MCl_4^- change significantly. The Cl–M–Cl bond angle that is around 60^0 changes to 109^0. Unlike in MCl_n ($n \leq 3$) clusters, the charge on the metal atoms remains nearly the same in both anion and neutral clusters.

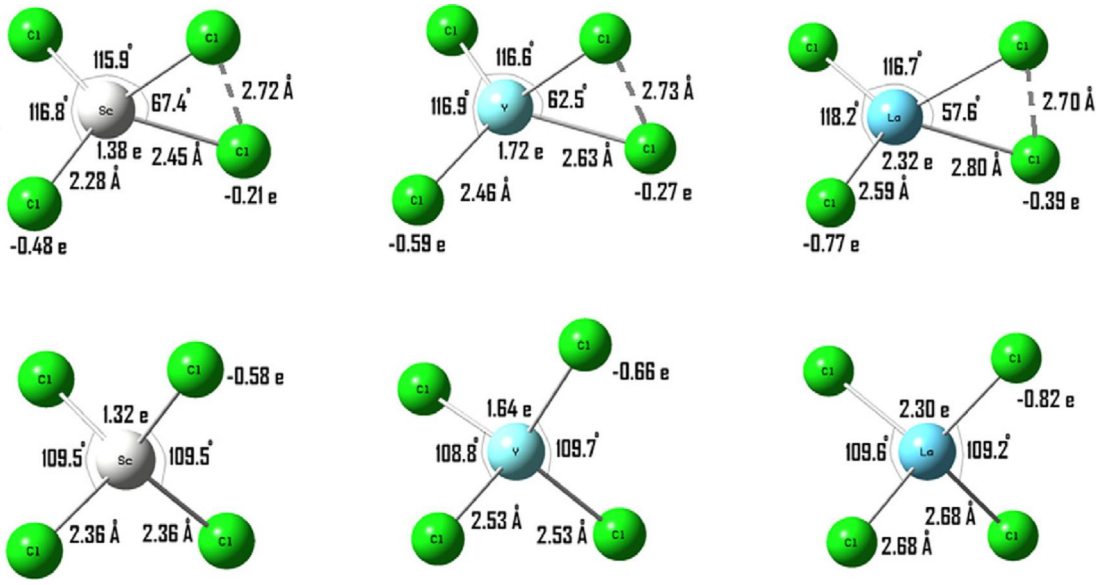

Figure 4. Structures of MCl_4 (top row) and MCl_4^- (bottom row) at (M = Sc, Y, La) B3LYP/SDD/6-311+G(3df).

Note that Sc, Y, and La atoms have a maximal valence of 3, and hence can accommodate at best three Cl atoms using the conventional bonding mechanism. The anion, having sufficient electrons form four two-center two-electron bonds and possesses tetrahedral geometry. Compared to the electron deficient bonds in neutral, the bond lengths of MCl_4^- are shorter. The extra electron in the anionic clusters is distributed uniformly over four Cl atoms (see the NBO charges in Fig. 4). This has dramatic effect on the electron affinities which are shown in Table 5.

Table 5: EA of MCl_4 and VDE of MCl_4^- (M = Sc, Y, La).

Method/Basis set	$ScCl_4$		YCl_4		$LaCl_4$	
	EA (eV)	VDE (eV)	EA (eV)	VDE (eV)	EA (eV)	VDE (eV)
B3LYP/SDD/6-311+G(d)	6.11	6.35	6.21	6.47	5.99	6.48
B3LYP/SDD/6-311+G(3df)	5.96	6.32	6.03	6.39	5.90	6.43

The vertical detachment energies (and electron affinities) of $ScCl_4$, YCl_4, and $LaCl_4$ calculated at the B3LYP level of theory with SDD/6-311+G(3df) basis sets are respectively 6.32 (5.96), 6.39 (6.03) and 6.43 (5.90) eV. The corresponding experimental values are 7.14 (6.84), 7.31 (7.02) and 7.38 (7.03) eV [63, 64]. We note that the calculated values are about 1 eV smaller than the corresponding experimental values. This is mainly attributed to the inadequate electron correlation in density functional theory. Recently Dixon and coworkers [65,66] incorporated various corrections to get highly reliable electron affinities of metal hexafluoride. Besides extrapolating to complete basis set at CCSD(T), additional corrections for relativistic effect and spin orbit coupling were included in their approach.

We note that these electron affinities are not only substantially larger than those seen in MCl_n ($n \leq 3$) clusters, but also they are larger than that of Cl atom which is 3.62 eV. Thus, these clusters can be identified as superhalogens. As in the case of MCl_3, higher spin states of both neutral and anion are higher in energy. The quartet states of neutral MCl_4 are 3.73, 4.12 and

4.32 eV higher in energy than the doublet ground states for M = Sc, Y and La. The triplet states of the corresponding anions are higher than the singlet ground states by 4.29, 4.61 and 4.64 eV.

3.2.5 MCl_5 (M= Sc, Y, La)

We have examined the possibility of whether a fifth Cl atom can be attached to both neutral and anion MCl_4 clusters since further addition of Cl can only worsen the electron deficiency nature of neutral MCl_4.We found that this is indeed possible and in Fig. 5 we provide the geometries of neutral and anionic MCl_5 (M = Sc, Y, La) clusters. The equilibrium geometry of neutral MCl_5 clusters show that three of the Cl atoms are chemically bound, while two of them form a molecular-like structure and are weakly coordinated to the MCl_3 portion of the cluster. In the anion, the bond between the molecularly coordinated chlorine atoms break and all the five Cl atoms are chemically bound.

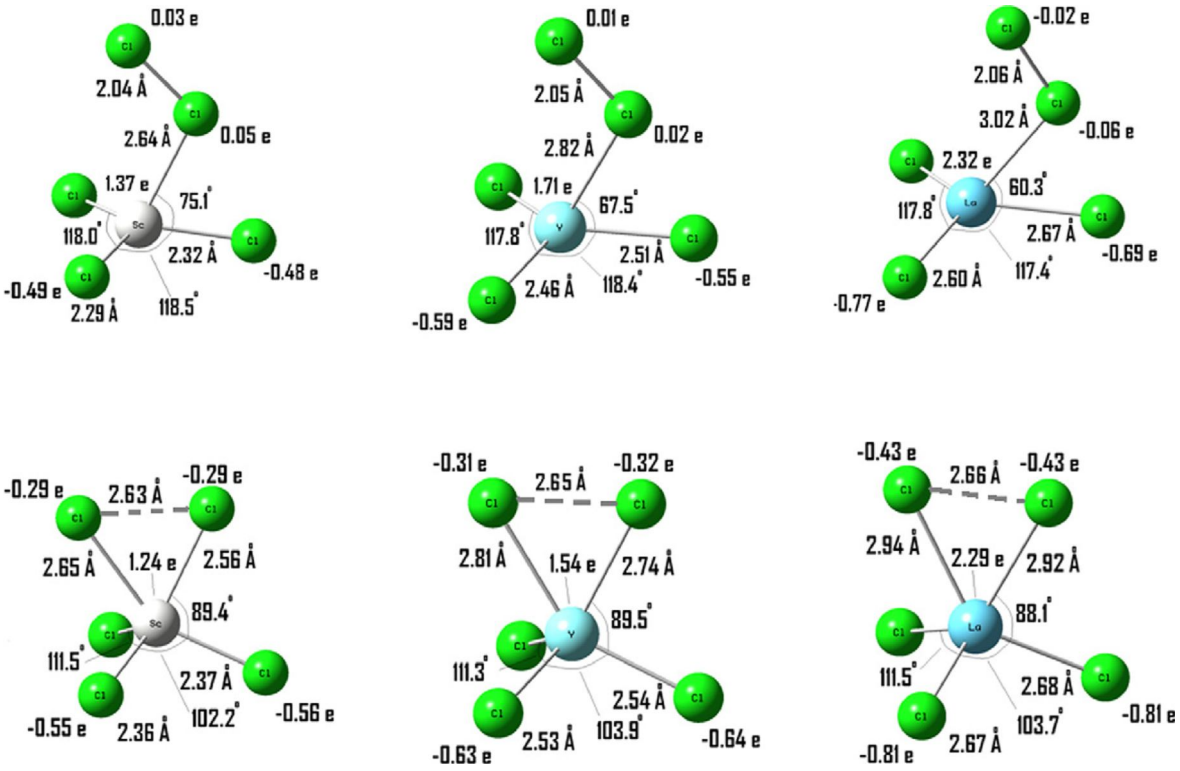

Figure 5. Structures of MCl_5 (top row) and MCl_5^- (bottom row) (M = Sc, Y, La) at B3LYP/SDD/6-311 + G(3df).

Despite our best efforts, which includes optimization by calculating the force constant at every step, a small imaginary frequency of -10 cm^{-1} for YCl_5^- and -24 cm^{-1} for $LaCl_5^-$ could not be eliminated at the B3LYP/SDD/6- 311+G(3df) level of theory. This imaginary vibration mode appears to be spurious but involves the side to side wagging of the two chlorine atoms at the top.

The preferred spin multiplicities of neutral and anionic MCl_5 clusters are respectively singlets and doublets. The triplet states of neutral MCl_5 clusters are 0.44, 0.33 and 0.30 eV higher in energy than the corresponding singlet states for Sc, Y, and La, respectively.

This marginal increase in energy is remarkable from the point of view of chemical bonding since the energies of triplet MCl_3 (see above) and Cl_2 (1.51 eV at B3LYP/6-311 + G* level) are quiet high. The doublet states of the anions are lower in energy than the quartet states by 4.04, 4.59 and 4.61 eV for Sc, Y, and La, respectively.

In Table 6 we provide the calculated vertical detachment energies and electron affinities of $ScCl_5$, YCl_5 and $LaCl_5$ clusters.

Table 6: EA of MCl_5 and VDE of MCl_5^- (M = Sc, Y, La).

Method/Basis set	**$ScCl_5$**		**YCl_5**		**$LaCl_5$**	
	EA (eV)	**VDE (eV)**	**EA (eV)**	**VDE (eV)**	**EA (eV)**	**VDE (eV)**
B3LYP/SDD/6-311+G(d)	5.35	6.29	5.61	6.46	5.53	6.49
B3LYP/SDD/6-311+G(3df)	4.98	6.21	5.22	6.34	5.17	6.46

Note that the electron affinities are larger than that of the Cl atom, and hence these clusters can also be classified as superhalogens. However, they are smaller than those in MCl_4 clusters (see Table 5). More interestingly, we note that there is significant difference between VDE and EA values. This arises due to considerable difference between the structures of the anions and their neutrals. No experimental results are available to compare with our calculated results.

3.3 Summary of the above calculations

Using density functional theory and generalized gradient approximation for exchange and correlation potential we have systematically studied the equilibrium structure, stability, electronic structure, vertical detachment energies and electron affinities of $ScCl_n$, YCl_n, and $LaCl_n$ (n = 1–5) clusters. For a given Cl composition our results are similar for Sc, Y and La. However, results vary strongly as Cl atoms are attached successively. In neutral MCl_n clusters, chlorine atoms are bound chemically for $n \leq 3$. In neutral MCl_5 clusters two of the Cl atoms bind weakly in a quasi-molecular fashion while the other three bind chemically. In MCl_4 clusters, on the other hand, two of the Cl atoms tend to be much closer than the others. In the anionic MCl_n clusters all Cl atoms bind chemically until $n \leq 4$. The partial bond between two Cl atoms in MCl_4 breaks once an extra electron is attached.

In Fig. 6 we summarize the stability of the neutral and anionic MCl_n clusters against fragmentation to chlorine atom or molecule.

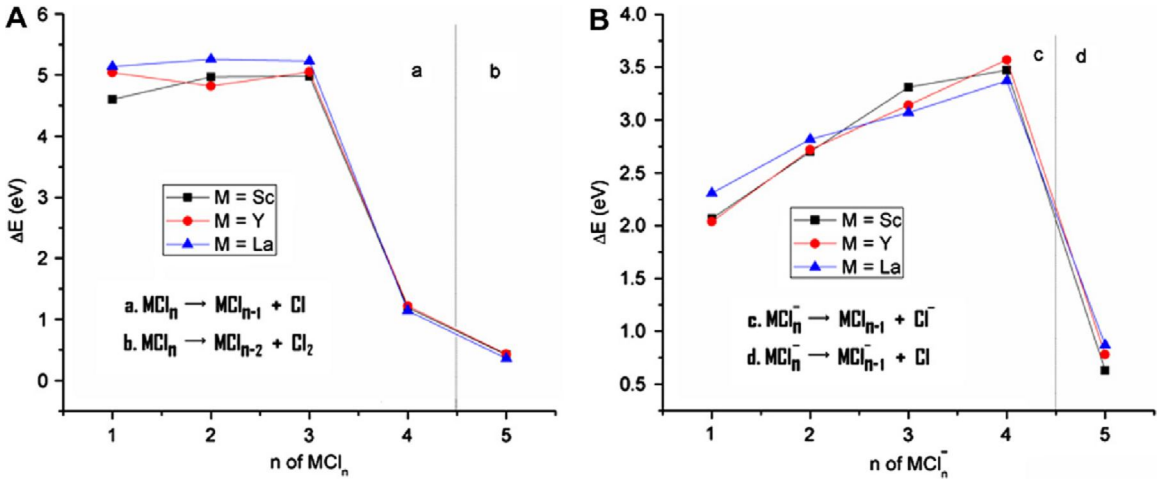

Figure 6. Lowest unimolecular decomposition energies at B3LYP/SDD/6-311+G(3df) level for (A) MCl_n (B) MCl_n^-

This is studied by calculating the fragmentation energies as defined below:

$$\Delta E_{atomic} = E[MCl_{n-1}] + E[Cl] - E[MCl_n]$$

$$\Delta E_{molecular} = E[MCl_{n-2}] + E[Cl_2] - E[MCl_n]$$

In the case of the anion, we calculate these energies using the equations,

$$\Delta E_{atomic} = E[MCl_{n-1}] + E[Cl^-] - E[MCl_n^-]$$

$$\Delta E_{atomic} = E[MCl_{n-1}^-] + E[Cl] - E[MCl_n^-]$$

$$\Delta E_{molecular} = E[MCl_{n-2}^-] + E[Cl_2] - E[MCl_n^-]$$

Here, the extra electron can be carried by either the Cl atom or the MCl_{n-1} cluster. The preferred path corresponds to the channel for which ΔE_{atomic} is lower.

The lowest fragmentation energies for both neutral and anion MCl_n clusters are shown in Figure 6(A) and (B) respectively. As can be seen, up to n = 3 the lowest path for fragmentation

for neutral clusters is by ejecting a Cl radical. About 5 eV of energy is required for breaking the MCl bond indicating that 2c-2e M—Cl bond is preferred over 2c-2e Cl—Cl bond. However, being electron deficient, the energy required to expel a Cl atom is drastically reduced for MCl_4. The preferred decomposition path for MCl_5 is to Cl_2 and MCl_3.

Given the high electron affinity of Cl, the preferred decomposition path for the MCl_n^- anions is by ejecting a Cl^- ion. This is the preferred path until n = 4. It may be noted that despite the high electron affinity of Cl, decomposition to Cl^- is endothermic, a consequence of the strong M—Cl bond. Because of the extraordinary stability of MCl_4^- the lowest decomposition path for MCl_5^- is to MCl_4^- and Cl.

The electron affinity of MCl_n clusters are plotted in Figure 7 as a function of Cl content. The EA values increase marginally until the valence of the metal atoms is consumed which in this case are three. Beyond that the EA values rise sharply indicating the onset of superhalogen behavior.

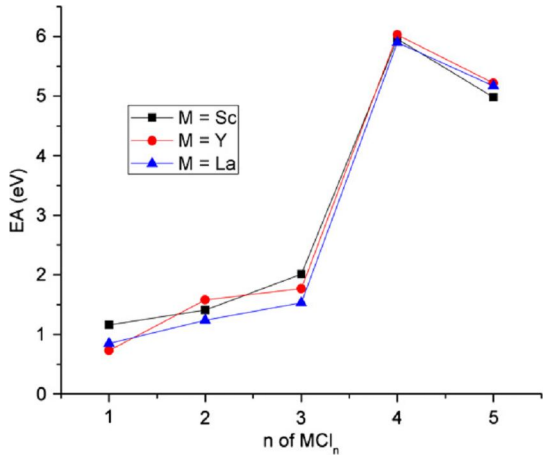

Figure7. Electron affinities of MCl_n (M = Sc, Y, La) at B3LYP/SDD/6-311 + G(3df).

The small increase in electron affinities for $n \leq 3$ and its abrupt increase at $n = 4$ is consequence of how the extra electron's charge is distributed. These are summarized in Figure 8. We note that for $n \leq 3$, the extra charge in the MCl_n^- clusters goes to the metal atom site and hence the electron affinities do not change much. However for $n \geq 4$, the extra charge is distributed over the Cl atoms and hence the electron affinity rises sharply.

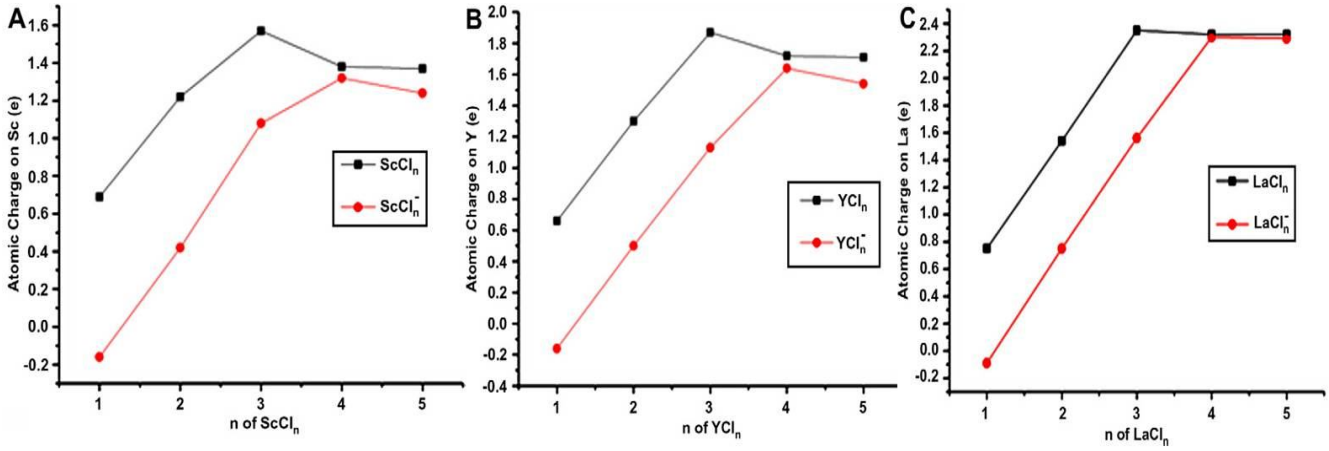

Figure 8. NBO atomic charges at B3LYP/SDD/6-311 + G(3df) level on metal atom in MCl_n series; (A) M = Sc, (B) M = Y, and (C) M = La.

Chapter 4

Computational Procedure, Results and Discussion Of Singly and Doubly Charged Anions of Metal Chloride and Pseudohalogen Clusters

4.1 Validation of Computational Procedure

All calculations have been carried out using density functional theory (DFT) with B3LYP hybrid functional for exchange and correlation (XC) potential [67, 68]. The accuracy of the DFT-based results is verified by carrying selected calculations using other *ab initio* quantum-chemical methods such as MP2 (second order Moller-Plesset Perturbation), CCSD(T) (Coupled Cluster with single, double excitations, and perturbative treatment of triple excitations) and comparing our results with available prior theoretical [69-72] and experimental [73-75] results. In all our calculations we have used 6-311++G(3df) basis sets which are known to provide excellent agreement between calculated and experimental results [76-79]. All other procedures are similar to that mentioned previously in section 3.1.

4.2 Results

In the following section A, we discuss the structure, stability, and spectroscopic properties of neutral, singly charged and doubly charged anions of $NaCl_n$ ($n \leq 3$), $MgCl_n$ ($n \leq 4$) and $AlCl_n$ ($n \leq 5$) clusters. Similar results where the Cl atoms are replaced by pseudohalogen are described in section B.

4.2.A Metal-Chloride Clusters MCl_n (M=Na, Mg, Al):

(i) $NaCl_n$ ($n \leq 3$)

Equlibrium Geometries:

In Figure.9 we provide the ground state optimized geometries of neutral, singly and doubly charged anions of $NaCl_n$ ($n \leq 3$) clusters. The bond lengths and NBO charge are also given in the figure. The bond length of the anionic NaCl is elongated compared to that in the neutral. In the neutral $NaCl_2$, the number of the Cl atoms exceeds the valence of the Na atom, and therefore in accordance with VSEPR (Valence Shell Electron Pair Repulsion) theory it has a bent shape due to the presence of one lone pair of electrons. $NaCl_2^-$, on the other hand, becomes a linear chain as the electron deficiency of Cl atom is fulfilled by the addition of an extra electron.

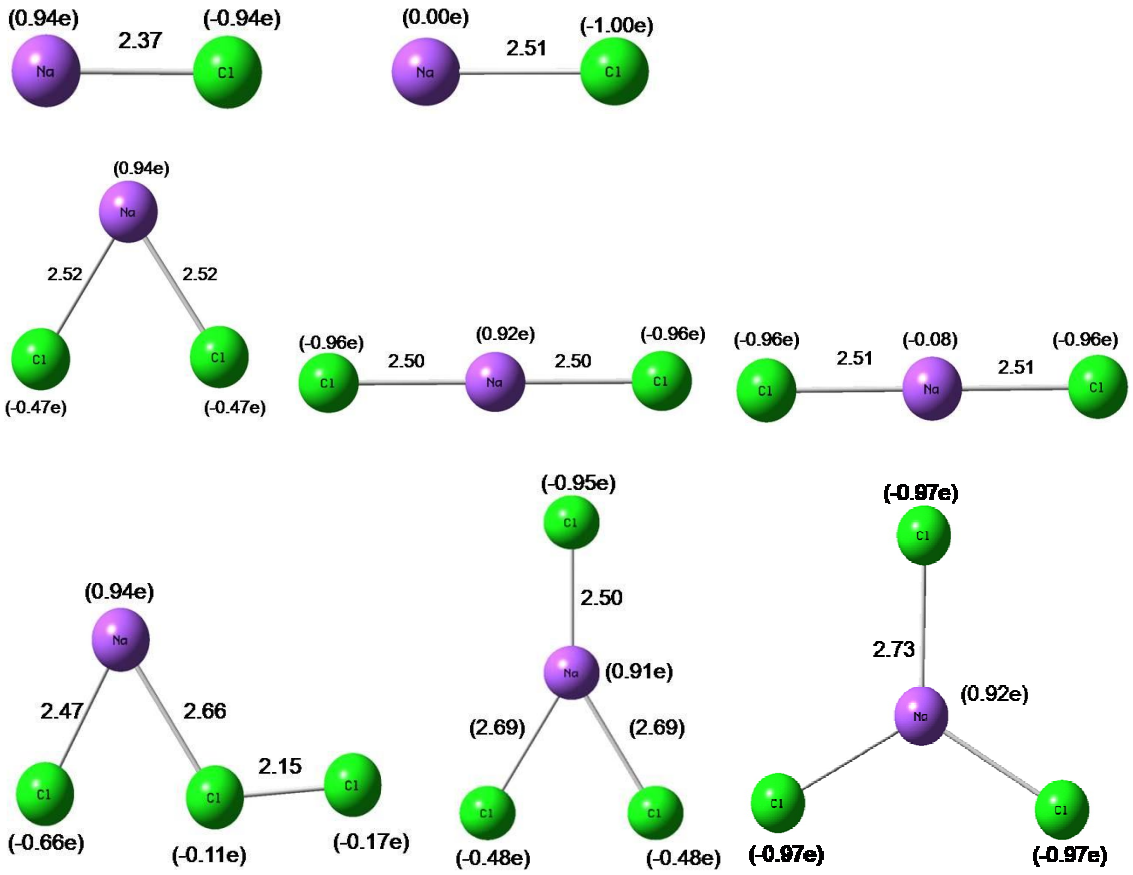

Figure 9: Optimized geometries of neutral (left), anionic (middle) and dianionic (right) $NaCl_n$ clusters at B3LYP/6-311++G(3df) level of theory.

The geometry of doubly charged $NaCl_2$ anion remains almost identical to that of $NaCl_2^-$, but found to be unstable as the repulsive interaction between the two extra electrons overwhelms the binding energy of the molecule. Its lack of stability will be discussed later by studying the fragmentation channel. In neutral $NaCl_3$ cluster, as Na can afford only one electron to the Cl atom, the other two Cl atoms binds quasi-molecularly with only one of them bound to the Na atom giving it an adduct type structure NaCl* Cl_2.

Note that the bond length between the chlorine atoms is 2.15 A° which is nearly similar to the bond length of the Cl_2 molecule (2.01 A°) calculated at the same level of theory as for this cluster. In $NaCl_3^-$, due to the availability of an extra electron, all the Cl-atoms bind chemically to the Na atom with two of the Cl atoms coming close together. As $NaCl_3^-$ is still an electron deficient cluster, it needs one more electron to fulfill the valence shell of all the Cl atoms. On addition of an extra electron to the anionic $NaCl_3$, the resulting dianion possesses a perfectly trigonal planar geometry and the extra electron is delocalized among all the Cl atoms.

Stability and Fragmentation:

The stability of neutral, anionic and dianionic clusters of $NaCl_n$ ($n \leq 3$) is determined by by calculating the least energy needed to fragment the cluster among all possible channels. We define these fragmentation energies as:

$$\Delta E^{neutral}(n) = E(NaCl_n) - E(NaCl_{n-m}) - E(Cl_m) \qquad m \leq 2 \qquad (1)$$

For calculating the corresponding fragmentation energies of the anion and dianion, one has to further consider which fragment carries the extra charge(s) or if the electron is autoejected. Thus, we define,

$$\Delta E^{1}_{anion}(n) = E(NaCl_n^-) - E(NaCl_{n-m}^-) - E(Cl_m) \qquad m \leq 2 \qquad (2)$$

$$\Delta E^{2}_{anion}(n) = E(NaCl_n^-) - E(NaCl_{n-m}) - E(Cl_m^-) \qquad m \leq 2 \qquad (3)$$

$$\Delta E^{3}_{anion}(n) = E(NaCl_n^-) - E(NaCl_n) - e^- \qquad (4)$$

$$\Delta E^{1}_{dianion}(n) = E(NaCl_n^{2-}) - E(NaCl_{n-m}^{2-}) - E(Cl_m) \qquad m \leq 2 \qquad (5)$$

$$\Delta E^{2}_{dianion}(n) = E(NaCl_n^{2-}) - E(NaCl_{n-m}^{-}) - E(Cl_m^-) \qquad m \leq 2 \qquad (6)$$

$$\Delta E\,^{3}{}_{dianion}(n) = \quad E(NaCl_n^{2-}) - E(NaCl_n^{-}) - e^{-} \qquad m \leq 2 \qquad (7)$$

The preferred channel for fragmentation and the corresponding energies are given in Table -7.

Table-7: Preferred fragmentation channels and energies of $NaCl_n$ clusters.

Neutral		**Mono-anion**		**Di-anion**	
Channel	ΔE (eV)	Channel	ΔE (eV)	Channel	ΔE (eV)
$NaCl \rightarrow Na + Cl$	4.06	$NaCl^{-} \rightarrow NaCl + e^{-}$	0.86		
$NaCl_2 \rightarrow NaCl + Cl$	1.31	$NaCl_2^{-} \rightarrow NaCl + Cl^{-}$	2.2	$NaCl_2^{2-} \rightarrow NaCl_2^{-} + e^{-}$	-1.99
$NaCl_3 \rightarrow NaCl + Cl_2$	0.54	$NaCl_3^{-} \rightarrow NaCl_2^{-} + Cl$	1.26	$NaCl_3^{2-} \rightarrow NaCl_2^{-} + Cl^{-}$ $\rightarrow NaCl_3^{-} + e^{-}$	-1.88 +0.55

We see that among neutral $NaCl_n$ clusters, NaCl is the most stable one as can be expected from ionic bonding argument. Among the mono-anion series, $NaCl_2^{-}$ is the most stable cluster due to its closed shell structure. The dianion of $NaCl_2$ is unstable against auto-ejection of an electron while the dianion of $NaCl_3$ is unstable against fragmentation into $NaCl_2^{-}$ and a Cl^{-} ion. However, the frequencies are positive indicating that these structures correspond to local minima in the potential energy surface. $NaCl_3^{2-}$ is metastable and can be seen in the experiment due to finite lifetime.

Electron Affinities (EA) and Vertical Detachment Energies (VDE*)*

The EAs of neutrals and VDEs of anions are calculated using DFT as well as MP2 and CCSD(T) methods. The VDEs are also calculated by the direct method i.e with using Outer Valence Green's Function (OVGF) method. The results are given in Table-8. We see that the results based on DFT agree with those with quantum chemical methods within 0.2 eV which currently is the accuracy of DFT-based methods.

Table-8: EA of $NaCl_n$ and VDE of $NaCl_n^-$ with 6-311++G(3df) basis set.

Method	**NaCl**		**$NaCl_2$**		**$NaCl_3$**	
	EA(eV)	**VDE(eV)**	**EA(eV)**	**VDE(eV)**	**EA(eV)**	**VDE(eV)**
B3LYP	0.86	0.91	4.58	4.98	4.21	5.64
MP2	0.68	0.71	4.78	5.85	3.92	6.16
CCSD(T)	0.69	0.72	4.68	5.74	3.98	5.78
OVGF		0.73		5.89		5.87

In case of NaCl cluster, the EAs and VDEs values are quite close to each other, which is consistent with minimal changes in the neutral and anionic geometries. On the contrary, the EA and VDE values are very different in $NaCl_2$ and $NaCl_3$ clusters due to the large difference between their corresponding geometries. The results compare well with earlier theoretical [90, 91] and experimental value [91] on $NaCl_2$ cluster. Note that the EA value of $NaCl_2$ is significantly higher than that of Cl, thus making it a superhalogen. Although $NaCl_3$ remains as a superhalogen, its EA is less than that of $NaCl_2$ due to its filled shell.

Charge Distribution:

One of the ways to understand the stability of $NaCl_n$ clusters and origin of the superhaogen behavior of $NaCl_2$ and $NaCl_3$ clusters is to analyze the charge distribution both in neutral and anionic states. This was done by calculating the charge on Na and Cl atoms as a function of n by using the natural bond orbital analysis. As seen from Figure.9 the charge on Na atom in neutral $NaCl_n$ clusters is same for $n \leq 3$ irrespective of how the Cl atoms are bound to it and the transferred charge is distributed among the Cl atoms. When an extra electron is added, it goes to the Na atom in NaCl, but in $NaCl_2$ and $NaCl_3$ the electron is distributed over the Cl atoms. Consequently, the electron affinity increases sharply. In $NaCl_2$ dianion, both the electrons reside on the Cl atom while Na remains electrically neutral. The electrostatic repulsion makes $NaCl_2$ dianion unstable. The case is different for $NaCl_3$. Here the charge on Na atom is nearly +1 and each of the Cl atoms carries an extra electron. The electrostatic interaction between Na^+ and Cl^- atoms provide metastability for the $NaCl_3$ dianion.

(ii) $MgCl_n$ ($n \leq 4$)

Equilibrium Geometries:

The ground state optimized geometries of neutral, singly and doubly charged clusters of $MgCl_n$ ($n \leq 4$) are displayed in Figure.10 with the bond lengths and the NBO charges. In $MgCl_2$ cluster, the charge on Mg in neutral $MgCl_2$ is +1.65e and the transferred charge is equally shared by both the Cl atoms. Consequently, it is a linear chain. However, on addition

of electrons to the neutral, the resulting anion and dianion have bent structures. The bond lengths are elongated due to the presence of a lone pair as per VSEPR theory.

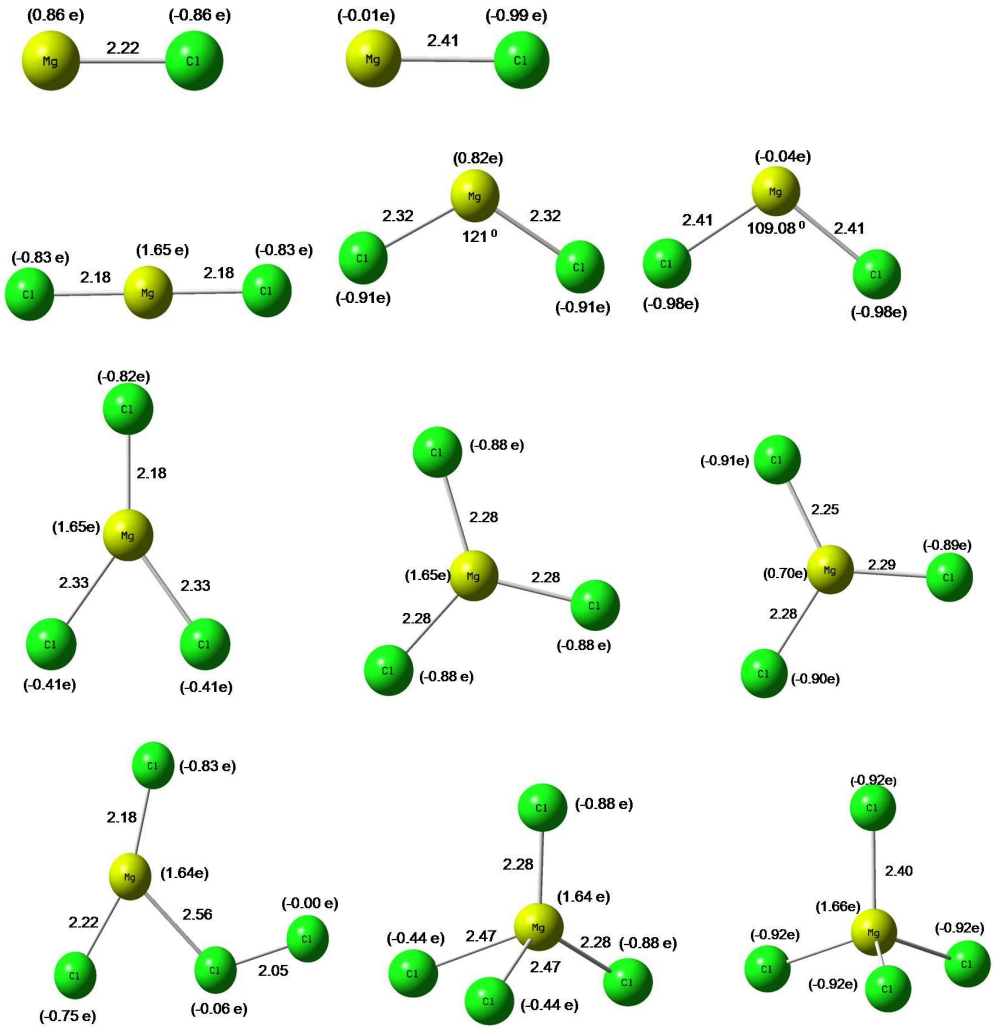

Figure 10: Optimized geometries of neutral (left), anionic (middle) and dianionic (right) $MgCl_n$ clusters at B3LYP/6-311++G(3df).

The energy difference between the anionic and dianionic cluster of $MgCl_2$ is found to be 2.76 eV. In $MgCl_3$ cluster, there is also a significant geometrical change between the mono-

anion and the neutral. In the neutral, as the number of Cl atoms exceeds the nominal valence of Mg atom, the bond lengths between Mg and two Cl atoms are stretched. On the other hand in $MgCl_3^-$ the third electron required to fill in the shells of three Cl atoms is supplied by the added electron giving it a perfect trigonal planar geometry. Upon addition of an extra electron the resulting dianion is again unstable as most of the charges are taken by the Mg atom and the large Coloumb repulsion dominates its binding energy. The energy difference between the anionic and dianionic $MgCl_3$ is found to be nearly 3 eV. In $MgCl_4$ cluster, the situation is very similar to that for $NaCl_3$. Due to its electron deficient nature, the two Cl atoms bind quasi-molecularly with a bond length 2.05 A° resulting in an adduct-like structure. Whereas in the anion, as Mg atom can only afford to lose two electrons the extra electron is distributed among all the Cl atoms and the bond between the quasi-molecularly bound Cl atoms breaks while the bonds between Mg and corresponding Cl atoms stretch to 2.47 A^o. As the anionic cluster needs one more electron to fulfill the valence of all the Cl atoms, the resulting dianion has a perfect tetrahedral geometry. Its energy is lowered by 1.07 eV as compared to its anion.

Stability and Fragmentation:

The stability of neutral, anionic and dianionic clusters of $MgCl_n$ are determined by calculating the fragmentation energies as defined in Eqs. (1) – (7). The preferred channels and the corresponding fragmentation energies are given in Table 9.

Note that energy needed to fragment $MgCl_2$ is the highest among the neutral clusters and hence is the most stable species. $MgCl_4$ dissociates into $MgCl_2$ and a Cl_2 molecule while the smaller clusters eject only a Cl atom.

Table-9: Preferred fragmentation channels and energies of $MgCl_n$ clusters**.**

Neutral		Mono-anion		Di-anion	
Channel	ΔE (eV)	Channel	ΔE (eV)	Channel	ΔE (eV)
$MgCl \rightarrow Mg + Cl$	3.21	$MgCl^- \rightarrow Mg + Cl^-$	1.13		
$MgCl_2 \rightarrow MgCl + Cl$	4.66	$MgCl_2^- \rightarrow MgCl_2 + e^-$	1.15	$MgCl_2^{2-} \rightarrow MgCl_2^- + e^-$	-2.76
$MgCl_3 \rightarrow MgCl_2 + Cl$	1.09	$MgCl_3^- \rightarrow MgCl_2 + Cl^-$	2.84	$MgCl_3^{2-} \rightarrow MgCl_3^- + e^-$	-2.97
$MgCl_4 \rightarrow MgCl_2 + Cl_2$	0.28	$MgCl_4^- \rightarrow MgCl_3^- + Cl$	0.99	$MgCl_4^{2-} \rightarrow MgCl_3^- + Cl^-$ $MgCl_4^- + e-$	-1.61 +1.07

On the other hand, $MgCl_3^-$ is the most stable cluster among the mono-anionic clusters. While $MgCl_2^-$ prefers to eject an electron, the other anions either eject a Cl^- atom for n =1 and 3 or a Cl atom for n = 4. The later is due to the fact that the $MgCl_3$ is a superhalogen which will be discussed later. All the dianions of $MgCl_n^{2-}$ are thermodynamically unstable against auto-ejection of an electron or Cl^-, but for n = 2-4, they belong to the local minima in the potential energy surface. Hence, these are metastable.

Electron Affinities (EA) and Vertical Detachment Energies (VDE):

The EAs of the neutrals and VDEs of the anions calculated using different theoretical models are given in Table 10. The experimental data is only available for the VDE of $MgCl_3^-$ [92]. The theoretical values are available only for $MgCl_3$ clusters [92, 93].

Table-10: EA of $MgCl_n$ and VDE of $MgCl_n^-$ with 6- 311++G(3df) basis set.

Method	MgCl		$MgCl_2$		$MgCl_3$		$MgCl_4$	
	EA(eV)	VDE(eV)	EA(eV)	VDE(eV)	EA(eV)	VDE(eV)	EA(eV)	VDE(eV)
B3LYP	1.61	1.74	1.15	1.87	5.43	5.74	4.85	6.40
MP2	1.30	1.45	1.0	1.69	5.75	6.62	4.61	6.95
CCSD(T)	1.53	1.68	1.52	1.72	5.65	6.53	4.65	6.58
OVGF		1.65		1.79		6.89		6.77
Expt						6.60**		

** **Ref** : Ben M. Elliott, Eldon Koyle, Alexander I. Boldyrev, Xue-Bin Wang, and Lai-Sheng Wang, J. Phys. Chem. A 2005, 109, 11560-11567

Note that results based on MP2 and CCSD(T) methods agree well with available experimental data. From our data, we found that the values of EAs and VDEs are quite similar for $MgCl_n$ clusters and it gradually increases as the number of Cl content increases. The EA values significantly increase for $MgCl_3$ and $MgCl_4$ which indicates the onset of superhalogen behavior. Note that the difference between EA and VDE is especially large for $MgCl_4$, around 2 eV. This due to a large geometry change (see Figure 10).

Charge Distribution:

In order to understand the nature of bonding, we analyzed the charge on Mg atom as a function of n, where n is the number of Cl atoms for neutral, anion and dianionic species using natural bond orbital analysis (NBO). The results are displayed in Figure 10. We found that in all the neutral clusters the bonding is basically ionic in nature. On addition of an electron to the neutral cluster, the charges prefer to reside on Mg atom for $n \leq 2$. When n exceeds the maximal valence of Mg atom ($n > 2$), the charge prefers to reside on the Cl atoms rather than on Mg which causes the EA to rise sharply. In neutral $MgCl_4$, the charge transfer is no longer possible and subsequently two Cl atoms bind quasi-molecularly. When one more electron is added to the anionic $MgCl_n$ cluster for $1<n < 3$, most of the charges are transferred to Mg atom. In $MgCl_4$ dianion the extra charge is delocalized among all the Cl atoms rather than staying on the Mg atom. This makes it stable against Coulomb repulsion due to its high binding energy. It can be noted from Fig.2 that the charges in the neutral, anion and the dianion are nearly the same at $n = 4$.

(iii) $AlCl_n$ ($n \leq 5$)

Equilibrium Geometries:

The ground state optimized geometries of neutral, mono-anion of $AlCl_n$ (n=1-5) and the dianions of $AlCl_n$ ($1< n \leq 5$) clusters are given in Figure.11 with their bond lengths and NBO charges. Unlike the clusters discussed before, the geometries of the neutral and the mono-anionic $AlCl_n$ clusters are very similar for $n \leq 5$. The differences are larger for $n \geq 4$ as Al is trivalent and each Cl atom needs an electron to close its shell.

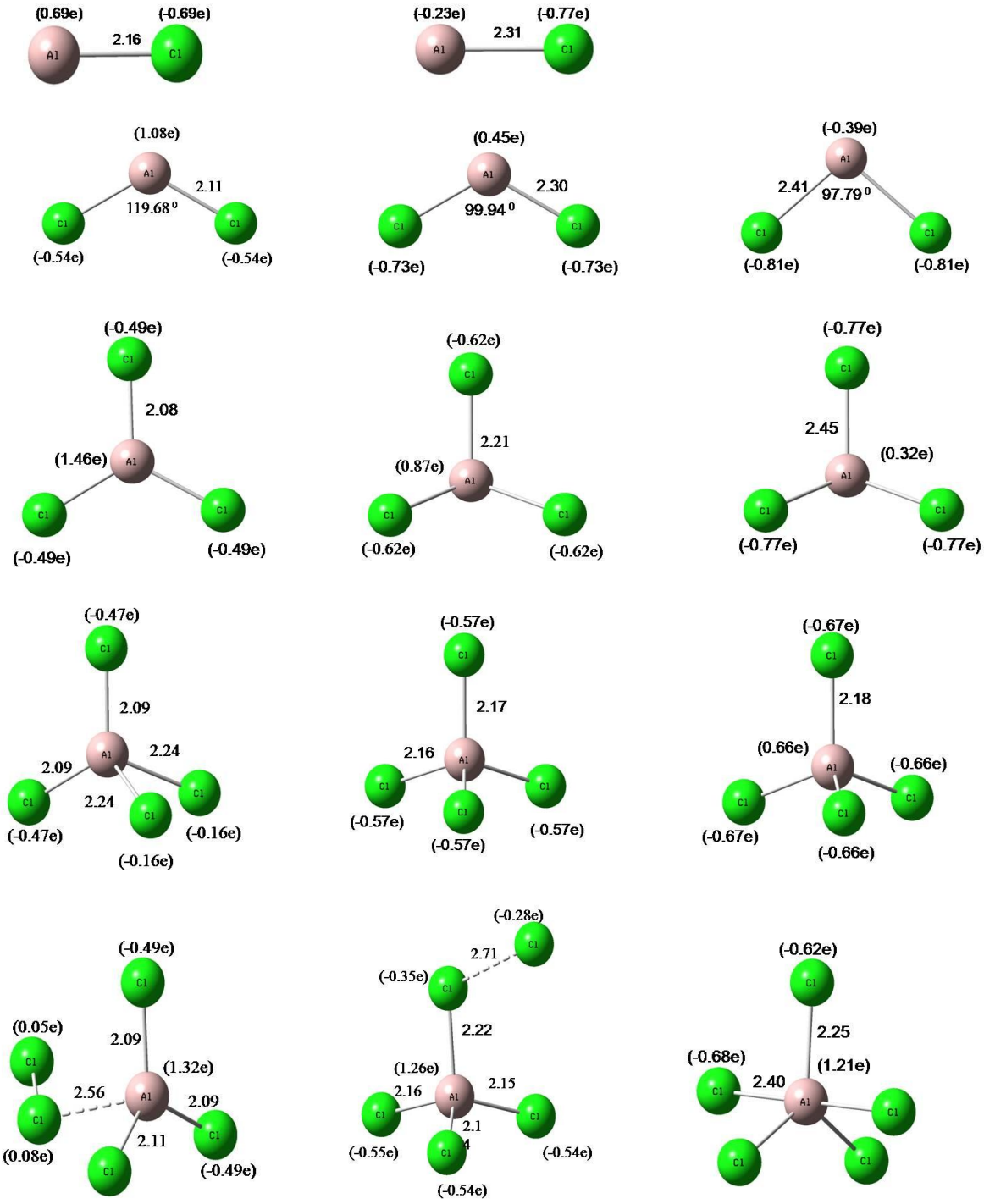

Figure 11: Optimized geometries of neutral (left), anionic (middle) and dianionic (right) $AlCl_n$ clusters at B3LYP/6-311++G(3df).

In the neutral $AlCl_4$ cluster, two of the Cl atoms bind to the Al atom with bond lengths of 2.24 Å while the other two have a shorter bond length of 2.09 Å. $AlCl_4^-$, on the other hand, has a perfect tetrahedral geometry as the extra electron can fill the shell of the Cl atom resulting in a closed shell structure. In the neutral $AlCl_5$ cluster, the two Cl atoms are bound in a quasi-molecular form having a bond length of 2.02 Å resulting in an adduct like structure $AlCl_3*Cl_2$ which is very similar to those seen in $NaCl_3$ and $MgCl_4$ clusters. In $AlCl_5^-$, the extra electron is not enough to fill the shells of all the Cl atoms. Consequently the quasi-molecular bond between the two Cl atoms in neutral $AlCl_5^-$ cluster is stretched to 2.71 Å. The geometries of dianions are similar as those of their corresponding mono-anionic clusters except for n = 5. $AlCl_5^{2-}$ forms a closed shell cluster and all the Cl atoms are chemically bound to the Al atom. It is the only stable species among all the dianions of $AlCl_n$ clusters against auto ejection of an electron.

Stability and Fragmentation:

The preferred fragmentation channel and corresponding dissociation energies of the neutral, anion and dianion of $AlCl_n$ clusters are given in Table 11.

We note that AlCl and $AlCl_3$ clusters are among the most stable neutral clusters. In the mono-anions, $AlCl_4^-$ is the most stable species. All dianions studied here are unstable against either auto-ejection of the electron or Cl^- ion. However, the frequencies associated with the dianion geometries are positive and hence they belong to minima in the potential energy surface, and are metastable.

Table-11: Preferred fragmentation channels and energies of $AlCl_n$ clusters.

Neutral		Mono-anion		Di-anion	
Channel	ΔE (eV)	Channel	ΔE (eV)	Channel	ΔE (eV)
$AlCl \rightarrow Al + Cl$	5.10	$AlCl^- \rightarrow AlCl + e^-$	0.19		
$AlCl_2 \rightarrow AlCl + Cl$	2.94	$AlCl_2^- \rightarrow AlCl + Cl^-$	1.62	$AlCl_2^{2-} \rightarrow AlCl_2^- + e^-$	-3.83
$AlCl_3 \rightarrow AlCl_2 + Cl$	4.80	$AlCl_3^- \rightarrow AlCl_3 + e^-$	1.44	$AlCl_3^{2-} \rightarrow AlCl_3^- + e^-$	-2.75
$AlCl_4 \rightarrow AlCl_3 + Cl$	0.88	$AlCl_4^- \rightarrow AlCl_3 + Cl^-$	3.08	$AlCl_4^{2-} \rightarrow AlCl_4^- + e^-$	-3.93
$AlCl_5 \rightarrow AlCl_4 + Cl$	0.18	$AlCl_5^- \rightarrow AlCl_4^- + Cl$	0.15	$AlCl_5^{2-} \rightarrow AlCl_4^- + Cl^-$ $\rightarrow AlCl_5^- + e-$	- 2.95 +0.21

Electron Affinities (EA) and Vertical Detachment Energies (VDE):

The EAs of the neutral and the VDEs of the anions calculated using different levels of theory are given in Table 12.

Table-12: EA of $AlCl_n$ and VDE of $AlCl_n^-$ with 6- 311++G(3df) basis set.

Method	AlCl		$AlCl_2$		$AlCl_3$		$AlCl_4$		$AlCl_5$	
	EA (eV)	VDE (eV)	EA (eV)	VDE (eV)	EA (eV)	VDE (eV)	EA (eV)	VDE (eV)	EA (eV)	VDE (eV)
B3LYP	0.19	0.30	2.36	2.91	1.44	2.67	5.88	6.17	4.71	6.50
MP2	-0.01	0.13	2.09	2.74	1.22	2.57	6.20	7.16	4.37	6.81
CCSD(T)	0.07	0.20	2.26	2.89	1.26	2.58	6.08	6.90	4.45	6.44
OVGF		0.21		2.91		2.73		7.04		6.95

No experimental values are available for these clusters. Note that the results obtained using DFT-B3LYP agrees well with those obtained from quantum chemical approaches. The EAs are small for AlCl. This is because the $3p^1$ electron of Al joins with the $3p^5$ shell of Cl making it a closed shell and leaving Al with a filled $3s^2$ shell. The electron affinity of $AlCl_2$ increases sharply, but decreases for $AlCl_3$. This odd-even effect is again the result of shell closure. $AlCl_4$ with an electron affinity of 5.88 eV is a superhalogen. Our results agree well with the theoretical value of the VDE of $AlCl_4^-$ cluster calculated by S Skurski and coworkers [94] using the OVGF method. The EA of $AlCl_5$ is higher than that of Cl, but smaller than that of $AlCl_4$ due to even number of electrons.

Charge Distribution:

The charge on neutral, anionic and dianionic clusters are displayed in Fig.3. Unlike in the case of $NaCl_n$ clusters, the charge on Al atom never reaches +3 irrespective of how many Cl atoms are attached to it. However, it increases from (+0.69e) in neutral AlCl to (+1.46e) in $AlCl_3$. This represents more covalent nature of the bonding. In $AlCl_4^-$ the extra charge is distributed among all the four Cl atoms and $AlCl_4$ becomes a superhalogen. The charges on the Cl atoms range from (0.47e) to (0.81e), except in the case of $AlCl_4$ and $AlCl_5$ where the quasi-molecular Cl atoms carry very little extra charge.

4.2.B. Metal-Cyanide MX_n (M=Na, Mg, Al and X= -CN or –NC) Clusters:

In the following section, we carried out a systematic study of psuedohalogen clusters. As the name suggest, psuedohalogens mimic the chemistry of halogen atoms and are composed of multi-atom species. They form (i) strong bound univalent radical, (ii) a singly charged anion, and (iii) a pseudohalogen-hydrogen acid, etc [80]

The term pseudohalogen was first introduced by Birckenback in 1925 [81] and further developed in a series of papers [82-84]. The purpose of choosing CN pseudohalogen is due to its high electron affinity (~ 4.05 eV) compared to Cl (~ 3.68 eV), calculated at the same level of theory. In addition, the resulting anions have very large electronic stabilities [85], due to which they are important in chemical synthesis and have versatile applications in the production of polyurethanes [86], a wide range of copolymers and abrasion-resistance polymers [87], semiconductor photoreceptors [88] and solid polymer electrolytes [89].

In the following we will discuss each cluster individually. In every cluster it is found that the bond length between N and C in all these clusters varies in the range (1.15-1.20 Å) which is very similar to the bond length between C-N (~ 1.17 Å) calculated at the same level of theory, which indicates that the species consisting of -NC functional group is bound to the metal atoms.

(i) NaX_n (X= -NC, $n \leq 3$)

In Figure.12, we provide the ground state optimized geometries of neutral, singly and double charged anion of NaX_n ($n \leq 3$) clusters along with bond lengths and NBO charges. All clusters have been studied with both –CN and –NC ligand attached to the metal atom. We found

that although the minimum energy geometries correspond to clusters when N-atom is bound to the metal atom, in most of the cases the cyanide and isocyanide groups are energetically nearly degenerate.

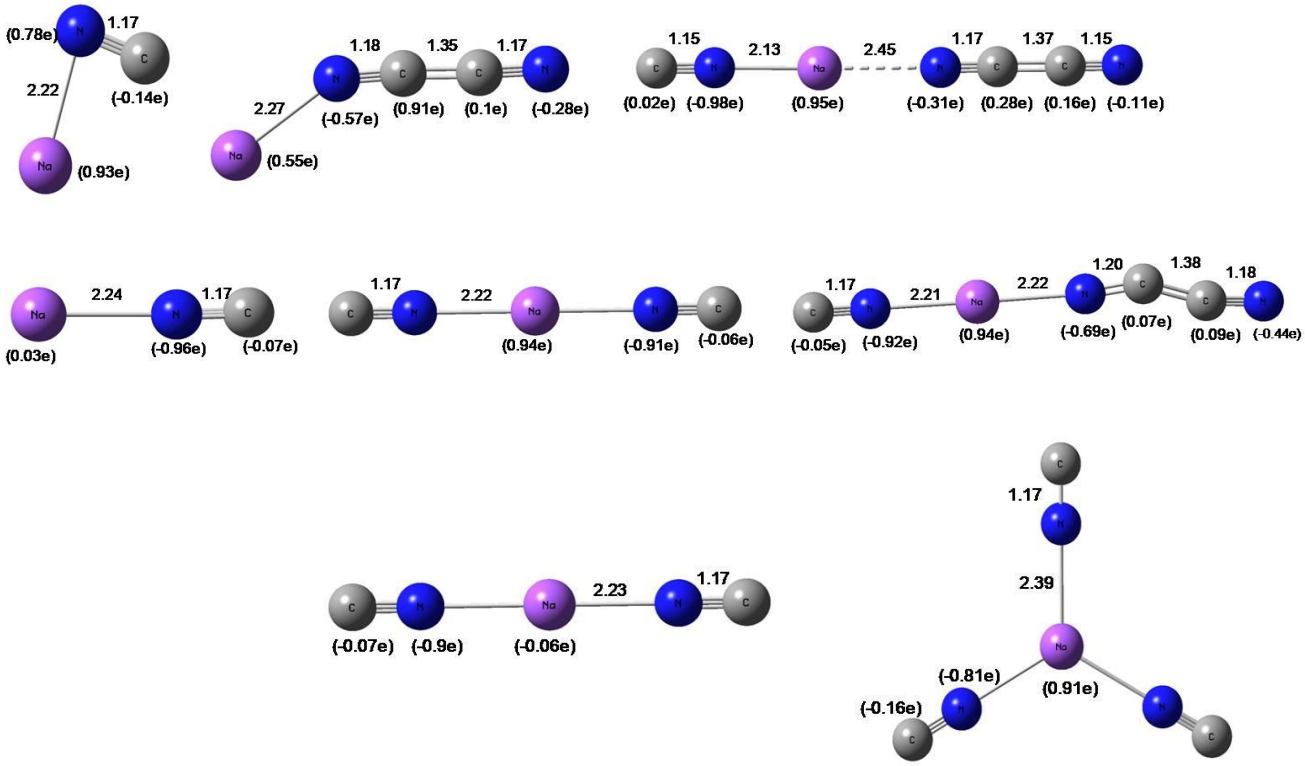

Figure 12: Optimized geometries of neutral (top), anionic (middle) and dianionic (bottom) of $Na(NC)_n$clusters at B3LYP/6-311++G(3df).

The geometries of CN pseudohalogens interacting with Na are similar to that of metal chloride clusters of Na except for the neutral NaNC and $Na(NC)_2$ and the anionic $Na(NC)_3$. When the number of ligand exceeds the valence of Na, the CN moieties dimerize. This can be seen in neutral $Na(NC)_2$ and $Na(NC)_3$ and in anionic $Na(NC)_3$. However on addition of extra

electrons to these clusters, the electron deficiency of the clusters can be overcome. Note that the geometry of the dianion of $Na(NC)_3$ is perfectly trigonal planar which is completely different from that of the anion and is dynamically stable. This will be explained later.

The preferred channel for fragmentation and the corresponding energies are given in Table 13.

Table-13: Preferred fragmentation channels and energies of $Na(NC)_n$ clusters.

Neutral		**Mono-anion**		**Di-anion**	
Channel	ΔE (eV)	Channel	ΔE (eV)	Channel	ΔE (eV)
$NaNC \rightarrow Na + NC$	4.32	$Na(NC)^- \rightarrow NaNC + e^-$	0.94		
$Na(NC)_2 \rightarrow Na + (NC)_2$	0.43	$Na(NC)_2^- \rightarrow NaNC + (NC)^-$	2.26	$Na(NC)_2^{2-} \rightarrow Na(NC)_2^- + e^-$	-1.94
$Na(NC)_3 \rightarrow NaNC + (NC)_2$	0.33	$Na(NC)_3^- \rightarrow Na(NC)^- + (NC)_2$	1.56	$Na(NC)_3^{2-} \rightarrow Na(NC)_2^- + (NC)^-$ $Na(NC)_3^- + e-$	-1.44 0.12

Among all the neutral clusters, NaNC is the most stable species due to its high fragmentation energy. While $Na(NC)_2$ and $Na(NC)_3$ prefer to dissociate by producing $(NC)_2$ dimer. In the anionic clusters, $Na(NC)_2^-$ is the most stable species among the anions. The dianion of $Na(NC)_2$ and $Na(NC)_3$ are metastable due to their positive frequencies. It can be noted that the fragmentation product of the dianions of $NaCl_n$ and $Na(NC)_2$ are similar, but its fragmentation energies are -1.88 eV and -1.44 eV respectively, which indicates that $Na(NC)_3$ dianion is more stable than $NaCl_3$ dianion.

Our results for the electron affinities (EA) of neutral and vertical detachment energy (VDE) of anion for $Na(NC)_n$ clusters are given in Table 14.

Table-14: EA of $Na(NC)_n$ and VDE of $Na(NC)_n^-$ with 6-311++G(3df) basis set**.**

Method	NaNC		$Na(NC)_2$		$Na(NC)_3$	
	EA(eV)	VDE(eV)	EA(eV)	VDE(eV)	EA(eV)	VDE(eV)
B3LYP	0.90	1.06	3.89	5.15	2.16	2.76
OVGF		0.88		5.86		2.20

The data show that both EA and VDE rise sharply at n=2 and drop at n=3. At n=2, the cluster is a superhalogen. Basically in superhalogens, the charge no longer goes to the metal atom. Instead, it is transferred to the electronegative ligand and the charges on the metal atom in both neutral and anion clusters are nearly same. This is not the case for neutral $Na(NC)_2$. This is due to the small electron affinity of NCCN dimer (~ 0.53 eV calculated at the same level of theory). For n=3 the geometries of both the neutral and the anion are quite similar (as shown in Fig.12). Due to the dimerization of CN there is a drop in the EA at n=3 and hence it does not behave as a superhalogen. (Its EA could have been high if the –NC ligands are not allowed to dimerize. But those clusters do not belong to a genuine minimum as is evidenced by an imaginary frequency). In case of dianion of $Na(NC)_2$, the negative charge is mostly transferred to Na in order to neutralize its positive charge while in the dianion of $Na(NC)_3$, the extra charges are distributed equally among all the ligands resulting in a perfect trigonal planar geometry. Due to this reason, it is more stable than that of its corresponding anion.

(i) MgX_n (X= -NC, n ≤ 4)

In Figure.13, we provide the ground state optimized geometries of neutral, singly charged and double charged anion of $Mg(NC)_n$ ($n \leq 4$) along with the bond lengths and NBO charges.

In these clusters, the N atom of CN preferentially binds to the central atom Mg due to its high electron negativity compared to that of C atom.

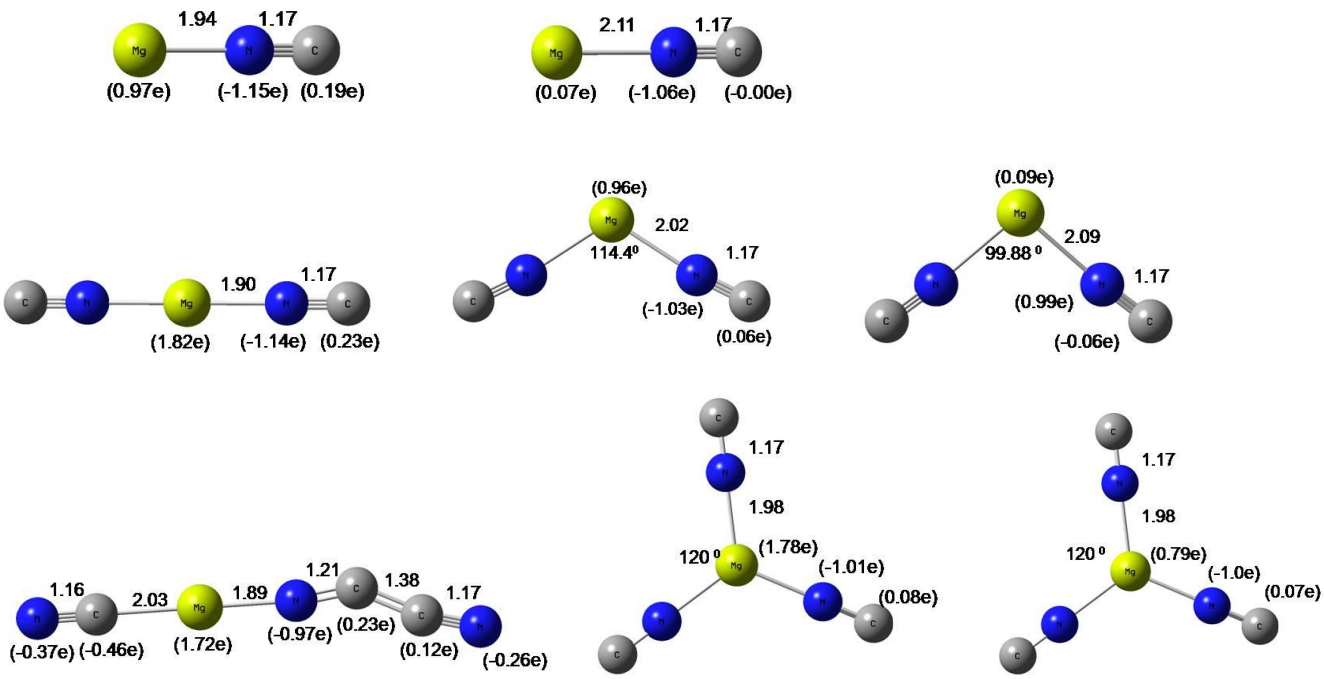

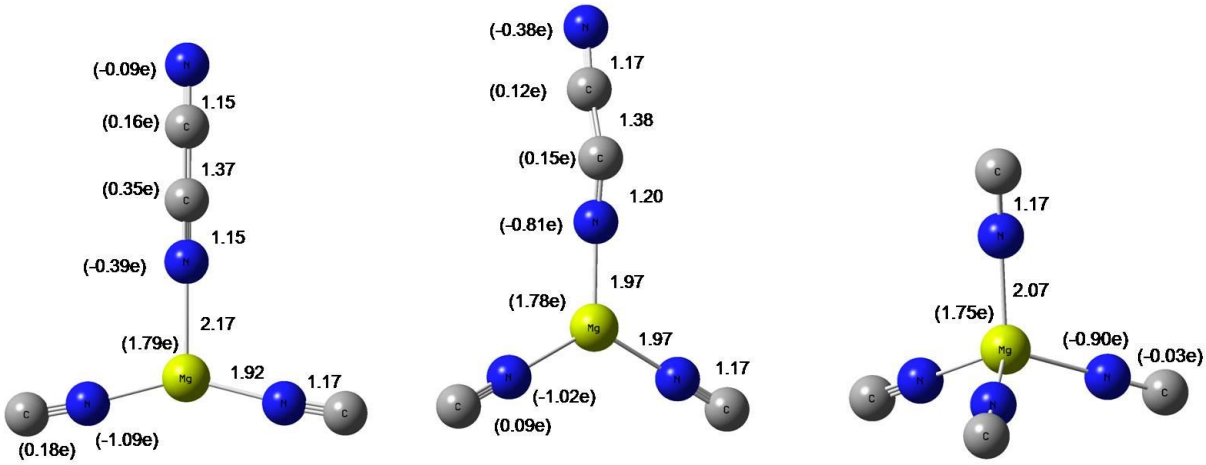

Figure 13: Optimized geometries of neutral (left), anionic (middle) and dianionic (right) of $Mg(NC)_n$ clusters at B3LYP/6-311++G(3df).

In MgNC cluster, both the geometries of neutral and anion are similar and the bonding is ionic in nature. As Mg can afford 2 electrons, the neutral $Mg(NC)_2$ is linear whereas both the anions and dianions are bent due to the lone pair of electron as per VSEPR theory. Whereas in case of $Mg(NC)_3$, the neutral geometry is very different than that of its anionic and dianionic counterpart. In the neutral cluster, due to electron deficiency, the two –NC ligands dimerize, whereas in $Mg(NC)_3^-$, the added electron along with the two valence electrons of Mg are enough to fill the shells of the three –NC ligands. Consequently, the geometry of $Mg(NC)_3^-$ is a perfect trigonal planar. The extra electron resides on the Mg atom to neutralize its positive charge. On the other hand, as Mg atom can afford maximum 2 electrons, the two –NC clusters dimerize in both neutral and anionic clusters of $Mg(NC)_4$. This is because the binding energy of $(NC)_2$ is

very high (~ 6.30 eV). In the dianion, all the –NC ligands are bound to Mg forming a perfect tetrahedral geometry, due to its closed shell structure.

The dianions of $Mg(NC)_n$ for $n \geq 3$ are thermodynamically unstable since the Coulomb repulsion between the extra electrons dominate the binding energies of the clusters.

The preferred channel for fragmentation and the corresponding energies are given in Table -15.

Table-15: Preferred fragmentation channels and energies of $Mg(NC)_n$ clusters.

Neutral		**Mono-anion**		**Di-anion**	
Channel	**ΔE (eV)**	**Channel**	**ΔE (eV)**	**Channel**	**ΔE (eV)**
$MgNC \rightarrow Mg + NC$	3.39	$Mg(NC)^- \rightarrow Mg + (NC)^-$	1.10		
$Mg(NC)_2 \rightarrow Mg + (NC)_2$	1.91	$Mg(NC)_2^- \rightarrow MgNC + (NC)^-$	2.41	$Mg(NC)_2^{2-} \rightarrow Mg(NC)_2^- + e^-$	-2.56
$Mg(NC)_3 \rightarrow MgNC + (NC)_2$	0.74	$Mg(NC)_3^- \rightarrow Mg(NC)_2 + (NC)^-$	3.46	$Mg(NC)_3^{2-} \rightarrow Mg(NC)_3^- + e^-$	-2.72
$Mg(NC)_4 \rightarrow Mg(NC)_2 + (NC)_2$	0.70	$Mg(NC)_4^- \rightarrow Mg(NC)_2^- + (NC)_2$	2.00	$Mg(NC)_4^{2-} \rightarrow Mg(NC)_3^- + (NC)^-$ $\rightarrow Mg(NC)_4^- + e^-$	-0.70 +0.93

Among all the neutrals, MgNC is the most stable species against fragmentation. At first, this may seem surprising since Mg is divalent. However, CN psuedohalogens gain considerable binding energy after dimerization (~ 6.30 eV). For the same reason all other neutral clusters prefer to dissociate by ejecting $(NC)_2$. Among the anions, $Mg(NC)_3$ is the most stable species. All anions except for n = 4 prefer fragmentation by ejecting a NC ion, whereas $Mg(NC)_4$ anion

prefers to dissociate into $Mg(NC)_2^-$ and $(NC)_2$. The negative charge resides on $Mg(NC)_2$ due to the small EA of $(NC)_2$ ligand. The dianion of $Mg(NC)_2$ and $Mg(NC)_3$ prefer to auto eject an electron and are highly unstable due to their large fragmentation energies. Whereas the dianion of $Mg(NC)_4$ is stable against auto ejection of an electron. This process liberates +0.93 eV of energy. However, it is found to be metastable against dissociation into $Mg(NC)_3^-$ and $(NC)^-$ and is thermodynamically more stable than that of its anionic counterpart.

The electron affinities (EA) of neutral and vertical detachment energy (VDE) of anion for $Mg(NC)_n$ clusters are summarized in Table 16.

Table-16: EA of $Mg(NC)_n$ and VDE of $Mg(NC)_n^-$ with 6- 311++G(3df) basis set.

Method	**MgNC**		**$Mg(NC)_2$**		**$Mg(NC)_3$**		**$Mg(NC)_4$**	
	EA(eV)	**VDE(eV)**	**EA(eV)**	**VDE(eV)**	**EA(eV)**	**VDE(eV)**	**EA(eV)**	**VDE(eV)**
B3LYP	1.76	1.91	1.64	2.44	5.29	6.21	2.93	3.83
OVGF		1.90		2.43		7.15		3.46

We found that there is a sudden rise of EA at n = 3 and hence $Mg(NC)_3$ is a superhalogen. There is a quite large energy difference in between EA and VDE values for n = 3 which is due to significant changes in the geometries of the neutral and anion. On addition of electron to the neutral clusters, most of the charges are transferred to Mg until n = 2. Beyond this it is distributed over the pusedohalogens. Due to this reason, the charges on the Mg atom, in both neutral and anion for $n \geq 3$ are found to be similar (as shown in Fig.13). It can also be noted that

the charges on Mg for n = 4 in neutral, anionic and dianionic clusters are similar. Whereas the EA as well as VDE drops in both neutral and anion, the –NC ligand dimerizes.

(i) AlX_n (X= -NC, n ≤ 5)

In Figure.14, we provide the ground state optimized geometries of neutral, singly charged and doubly charged anion of AlX_n (where n ≤ 5) along with the bond lengths and NBO charges.

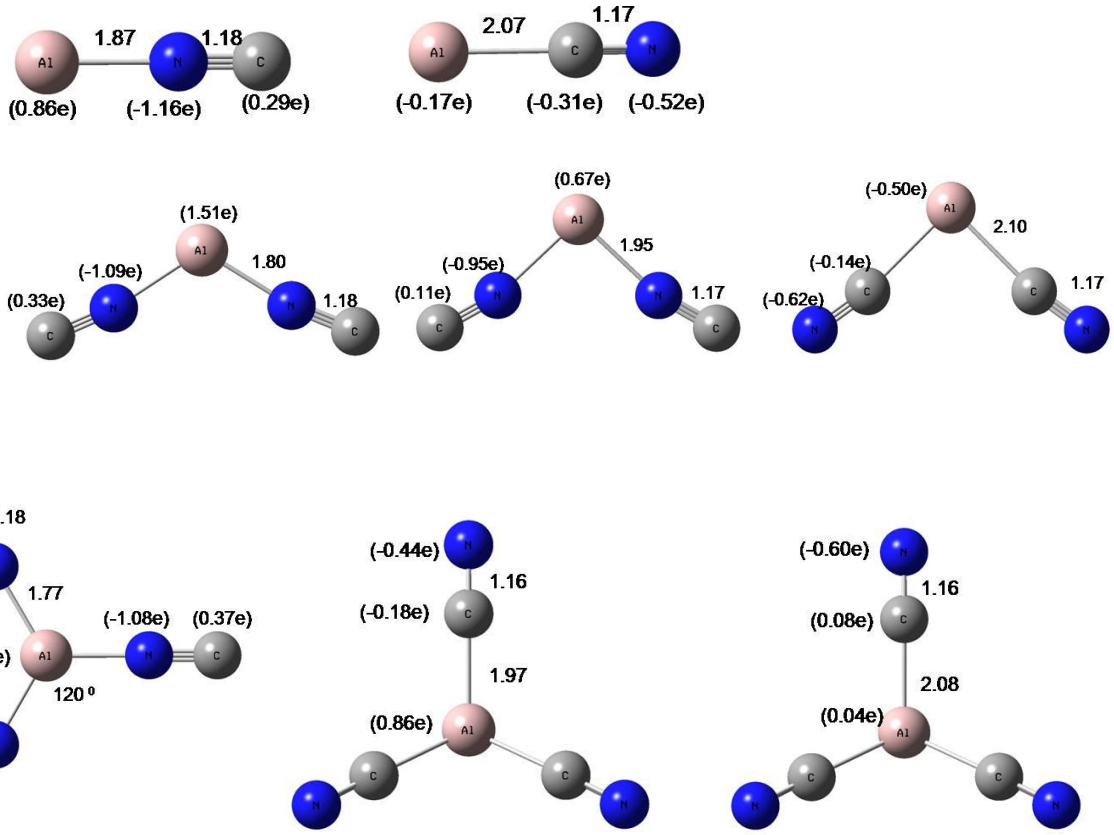

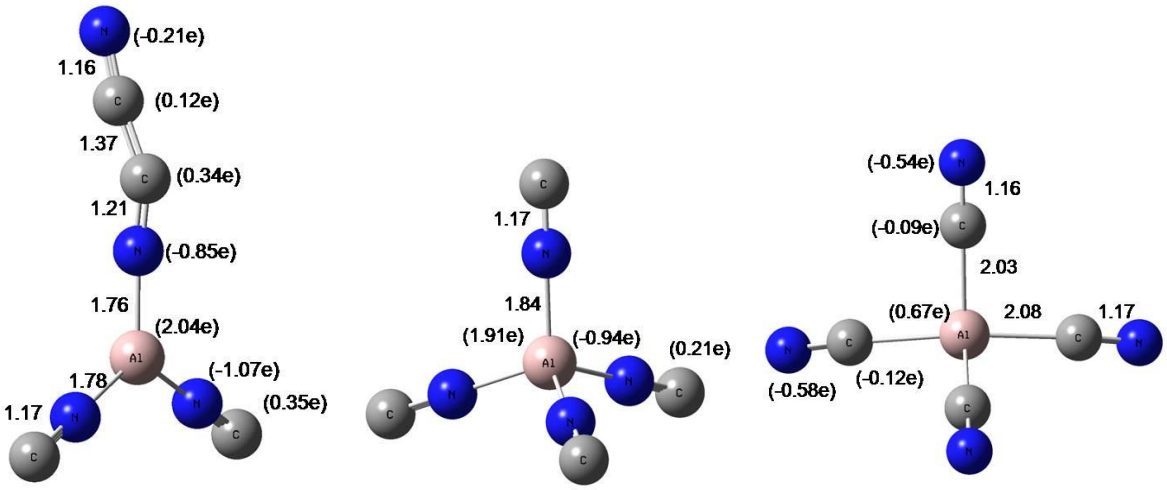

Figure 14: Optimized geometries of neutral (left), anionic (middle) and dianionic (right) of $Al(NC)_n$ clusters at B3LYP/6-311++G(3df).

These pseudohalogen clusters are very different as compared to all the Na and Mg clusters. In AlX cluster, the energies of the clusters are nearly degenerate (around 0.3 eV in neutral and 0.03 eV in anion) whether C or N atom is attached bound to the metal atom. The geometries are given based on the minimum energy structure. In AlX_2, due to the presence of lone pair of electron, the geometries of neutral, anion and dianion are bent in shape, while in the dianion, C atom is bound to Al rather than N. On the other hand, in AlX_3, the neutral has a very stable geometry as the 3 valence electrons of Al are shared by the ligands giving it a perfectly trigonal geometry. When an extra electron is added, C atom preferentially binds to Al in both the anion and dianion. As the Al-atom can at most provide 3 electrons for bonding, CN prefers to dimerize when the number of ligands exceed the maximal valence of Al. This can be seen from

the geometries of neutral AlX_n cluster. When the electron deficiency is fulfilled by adding an electron, the anion assumes tetrahedral symmetry and $Al(CN)_4^-$ is found to be most stable species. In the dianion, the C-atom is preferably binds to Al. For n=5, the neutral and anion have very similar geometry, while the dianion has a trigonal bipyramidal geometry. It is found to be the most stable species among all the dianions. Thus, we conclude that in all the neutral clusters N atom is preferably binds to Al due to its higher electronegativity compared to C. In the dianions, however, C atom binds to Al due to the availability of extra charge. The anions show different bonding mechanism than the neutral.

The preferred channel for fragmentation and the corresponding energies are given in Table 17.

Table-17: Preferred fragmentation channels and energies of AlX_n (X= -CN or –NC) clusters.

Neutral		**Mono-anion**		**Di-anion**	
Channel	ΔE (eV)	Channel	ΔE (eV)	Channel	ΔE (eV)
$AlNC \rightarrow Al + NC$	5.25	$AlCN^- \rightarrow AlCN + e^-$	0.85		
$Al(NC)_2 \rightarrow Al + (NC)_2$	2.25	$Al(NC)_2^- \rightarrow AlNC + (NC)^-$	2.05	$Al(CN)_2^{2-} \rightarrow Al(CN)_2^- + e^-$	-3.20
$Al(NC)_3 \rightarrow AlNC + (NC)_2$	2.23	$Al(CN)_3^- \rightarrow Al(CN)_3 + e^-$	2.65	$Al(CN)_3^{2-} \rightarrow Al(CN)_3 + e^-$	-2.25
$Al(NC)_4 \rightarrow Al(NC)_2 + (NC)_2$	0.38	$Al(NC)_4^- \rightarrow Al(NC)_3 + (NC)^-$	4.24	$Al(CN)_4^{2-} \rightarrow Al(CN)_4^- + e^-$	-3.35
$Al(NC)_5 \rightarrow Al(NC)_3 + (NC)_2$	-0.07	$Al(NC)_5^- \rightarrow Al(NC)_3^- + (NC)_2$	2.13	$Al(NC)_5^{2-} \rightarrow Al(NC)_4^- + (NC)^-$ $\rightarrow Al(CN)_5^- + e^-$	-1.55 +0.89

Among all the neutral clusters, AlNC is the most stable species having high fragmentation energy. All other neutral clusters prefer to dissociate by ejecting $(NC)_2$. In the case of anions, $Al(NC)_4^-$ is the most stable species due its superhalogen behavior. This will be explained shortly. While $AlCN^-$ and $Al(CN)_3^-$ auto eject an electron, $Al(NC)_5^-$ prefers to fragment to $Al(NC)_3^-$ and $(NC)_2$. On the other hand, the dianionic clusters for $n \leq 4$ auto eject an electron while, $Al(NC)_5^{2-}$ fragments into $Al(NC)_4^-$ and $(NC)^-$, since $Al(NC)_4^-$ is the most stable species among the anions. The dianion of $Al(NC)_5$ is found to be thermodynamically stable as compared to its anionic counterpart.

The EA and VDE of AlX_n clusters are mentioned in Table 18.

Table-18: EA of AlX_n (X= -CN or –NC) and VDE of AlX_n^- with 6- 311++G(3df) basis set.

Method	AlX		AlX_2		AlX_3		AlX_4		AlX_5	
	EA (eV)	VDE (eV)	EA (eV)	VDE (eV)	EA (eV)	VDE (eV)	EA (eV)	VDE (eV)	EA (eV)	VDE (eV)
B3LYP	0.57	0.86	2.81	3.35	2.38	3.53	5.84	6.87	3.44	4.58
OVGF		0.73		3.51		3.51		7.96		4.42

Due to the structural similarity between the neutrals and anions, there is a small energy difference between the EA and VDE. The charges are transferred to the Al atom till its valence is consumed i.e till n = 3. But as the number of ligands exceeds the valence of Al, the charges no longer reside on the Al atom and are distributed over the CN lignads. Consequently, the EA increases abruptly at n = 4. This is similar to what was seen in $AlCl_n$ clusters. The charge on Al

in neutral $Al(CN)_4$ is (+2.04e) whereas in the anion it is (+1.97e). In $Al(CN)_5$ clusters, due to dimerization of CN in both the neutral and anion, the value of EA drops. However, its dianion has a closed shell structure. Its energy is lower by ~ 2.7 eV from that of its anion, thus making it stable.

Chapter 5

Conclusion

A systematic theoretical study of the stability and spectroscopic properties of d^1 transition metals (Sc, Y and La) interacting with Cl atoms and simple metal atoms (Na, Mg, Al) interacting with Cl as well as CN moieties was carried out using gradient corrected density functional theory. The objective of my study was to find ways in which electronegative species with electron affinities much higher than those of Cl can be designed and synthesized. Our results led to the following conclusions:

(1) The d^1 transition metals (Sc, Y and La) behave as superhalogens when the number of Cl atoms exceeds the maximal valence of these atoms, namely 3.

(2) For simple metal atoms (Na, Mg, Al), superhalogen behavior is also observed when the number of Cl atoms exceed the normal valence of Na, Mg, and Al, namely 1, 2, and 3.

(3) CN moieties which are known as pseudohalogens can also form the building blocks of a new class of superhalogens. However, unlike halogens, they provide considerable challenge in designing superhalogens. First, CN can bind to a metal atom as cyanide (i.e. CN) or as an isocyanide (i.e. NC). Second, cyanogen which is a $(CN)_2$ dimer has very large binding energy compared to that of Cl_2. Consequently, as the number of CN moieties bound to a metal atom increases, the most stable configuration may not be the one where the CN moieties are bound individually, but rather structures where CN moieties dimerize and then bind to the metal atom.

In this case, they may not form superhalogens. This is what our systematic studies of CN moities bound to Na, Mg, and Al reveal. For Na, up to two CN moieties can be bound individually and $Na(CN)_2$ is a superhaolgen. Beyond this, CN moieties dimerize and the electron affinity of $Na(CN)_3$ drops below that of Cl. Similar systematic is seen for Mg and Al except the number of CN moities bound to these metal atoms that exhibit superhalogen behavior is 3 for Mg and 4 for Al.

The stability and electronic properties of the dianions were also studied in the gas phase. The results show that while some the dianions of the clusters studied here are stable against auto ejection of electron but they are all metastable against fragmentation. However, when compared between the halogens and pseudohalogens bound to a metal atom, the dianions composed of pesudohalogens are more stable than those composed of halogens. This is because the second electron in a dianion containing CN moieties finds a larger phase space to delocalize as opposed to those containing Cl. The results compared well with available experimental and theoretical data. The studies reveal that there are a number of ways where new superhalogens can be created and these can be useful in synthesizing new salts and oxidizing agents.

References:

[1] D. F. Hunt, G. C. Stafford, Jr., F. W. Crow, and J. W. Russell, Anal.Chem. 48, 2098 , (1976)

[2] F. Arnold, Nature London 284, 610, (1980).

[3] H. Hotop and W. C. Lineberger, J. Phys. Chem. Ref. Data 14, 731 , 1985.

[4] N. Bartlett, Proc. Chem. Soc. 218 ,1962.

[5] N. Bartlett, Angew. Chem., Int. Ed. 7 (1968) 433.

[6] G.L. Gutsev, A.I. Boldyrev, Chem. Phys. 56 (1981) 277.

[7] G.L. Gutsev, A.I. Boldyrev, Adv. Chem. Phys. 61 (1985) 169.

[8]G. L. Gutsev and A. I. Boldyrev, Chem. Phys. 56, 277 (1981).

[9] G. L. Gutsev and A. I. Boldyrev, Adv. Chem. Phys. 61, 169 (1985).

[10] P. J. Hay, W. R. Wadt, L. R. Kahn, R. C. Raffenetti, and D. H. Phillips, J. Chem. Phys. 71, 1767 (1979).

[11] G. L. Gutsev and A. I. Boldyrev, Chem. Phys. Lett. 84, 352 (1981)

[12] G. L. Gutsev and A. I. Boldyrev, Chem. Phys. Lett. 101, 441 (1983).

[13] N. Bartlett, Angew. Chem. Int. Ed. Engl. 7, 433 (1968).

[14] M. Boring, J. H. Wood, and J. W. Moskowtiz, J. Chem. Phys. 61, 3800.

[15] R. N. Compton, in Negative Ions, edited by V. A. Esaulov Cambridge University Press, Cambridge, (1995).

[16] X.-B. Wang, C.-F. Ding, L.-S. Wang, A.I. Boldyrev, J. Simons, J. Chem. Phys. 110, (1999) 4763.].

[17] F. Wudl, Acc. Chem. Res. 17, 227,1984].

[18] G.L. Gutsev, P. Jena, R.J. Bartlett, Chem. Phys. Lett. 192 (1998) 289.

[19] I. Anusiewicz, P. Skurski, Chem. Phys. Lett. 358 (2002) 426.

[20] I. Anusiewicz, M. Sobczyk, I. Dabkowska, P. Skurski, Chem. Phys. 291 (2003), 171.

[21] A.N. Alexandrova, A.I. Boldyrev, Y.-J. Fu, X. Yang, X.-B. Wang, L.-S. Wang, J. Chem. Phys. 121 (2004) 5709.

[22] S. Smuczynska, P. Skurski, Chem. Phys. Lett. 452 , (2008) 44.

[23] Sikorska, S. Smuczynska, P. Skurski, I. Anusiewicz, Inorg. Chem. 47 (2008), 7348.

[24] I. Anusiewicz, Aust. Chem. 61 (2008) 712.

[25] G.L. Gutsev, B.K. Rao, P. Jena, X.-B. Wang, L.-S. Wang, Chem. Phys. Lett. 312, (1999) 598.

[26] M. Sobczyk, A. Sawicka, P. Skurski, Eur. J. Inorg. Chem. (2003) 3790. 20,21.

[27] J. Yang, X.-B. Wang, X.-P. Xing, L.-S. Wang, J. Chem. Phys. 128 (2008) 201102.

[28] X. Yang, X.-B. Wang, L.-S. Wang, S. Niu, T. Ichiye, J. Chem. Phys. 119 (2003), 8311 22,23.

[29] Dougherty, R. C. J. Chem. Phys. 1969, 50, 1896.

[30] A. P. Bruins, T. R. Covey, and J. D. Henion, Anal. Chern. 59, 2642(1987).

[31] W. P. M. Maas and N. M. M. Nibbering, Int. J. Mass Spectrom. Ion Phys. 88, 257 (1989).

[32] H.-G. Weikert and L. S. Cederbaum, J. Chem. Phys., Vol. 99, No. 11, 1 December 1993.

[33] K Scheller and L S Cederbaum, J. Phys. B: At. Mol. Opt. Phys. 25 (1992) 2257-2265.,

[34] Andreas Dreuw and Lorenz S. Cederbaum, Chem. Rev. 2002, 102, 181-200.

[35] X-L. Zhao and A. E. Litherland, PHYSICAL REVIEW A 71, 064501, 2005.

[36] Roy Middleton and Jeff Klein, PHYSICAL REVIEW A, VOLUME 60, NUMBER 5,1999.

[37] H. G.; Cederbaum, L. S.; Tarantelli, F.; Boldyrev, A. I. Z. Phys. D-Atoms, Molecules, Clusters 1991, 18, 229.

[38] Weikert, H. G.; Cederbaum, L. S. J. Chem. Phys. 1993, 99, 8877.

[39] Koch, W.; Holthausen, M. C.; A Chemist's Guide to Density Functional Theory; Weinheim; New York : Wiley-VCH; 2001.

[40] Born, M.; Oppenheimer, J. R. Ann. Physik 1927, 79, 361.

[41] Hartree, D. R. Proc. Cambridge Phil. Soc. 1928, 24, 89.

[42] Szabo, A.; Ostlund, N. S.; Modern Quantum Chemistry: Introduction to Advanced Electronic Structure Theory; Macmillan, New York; 1982.

[43] Fock, V. Z. Physik 1928, 48, 73.

[44] Slater, J. C. Phys. Rev. 1951, 81, 385.

[45] Hohkenberg, P.; Kohn, W. Phys. Rev. B 1964, 136, B864.

[46] Kohn, W.; Sham, L. J. Phys. Rev. 1965, 140, A1133.

[47] Vosko, S. H.; Wilk, L.; Nusair, M. Canadian. J. Phys. 1980, 45, 566.

[48] Becke, A. D. Phys. Rev. A 1988, 38, 3098.

[49] Becke A. D., J. Chem. Phys., 1993, 98, 5648.

[50] Perdew J. P., in *Electronic Structure of Solids*, edited by P. Ziesche and H. Eschrig, Academic Press, Verlag, Berlin, 1991.

[51] Lee C.; Yang, W.; Parr, R. G.; *Phys. Rev. B* 1988, *37*, 785

[52] Slater, J. C. *Phys. Rev*. 1930, *35*, 210.

[53] Boys, S. F. *Proc. R. Soc. (London) A* 1950, *200*, 542.

[54] A.D. Becke, Phys. Rev. A 38 (1998) 3098.

[55] J.P. Perdew, Y. Wang, Phys. Rev. B 45 (1991) 13244.] for the GGA and B3LYP.

[56] A.D. Becke, J. Chem. Phys. 98 (1993) 5648., Ref: P.J. Stephens, F.J. Devlin, C.F. Chabalowski, M.J. Frisch, J. Phys. Chem. 98 (1994), 11623.

[57] M.J. Frisch et al., GAUSSIAN 03, Revision D.02, Gaussian Inc., Wallingford, CT, 2004.

[58] P. Lof, Elseviers's Periodic Table of the Elements, Elsevier Science Publishers B.V., Amsterdam, 1987.

[59] P. Lof, Elseviers's Periodic Table of the Elements, Elsevier Science Publishers B.V., Amsterdam, 1987.

[60] H. Fjellvag, P. Karen, Acta Chem. Scand. 48 (1994) 294.

[61] D.H. Templeton, G.F. Carter, J. Phys. Chem. 58 (1954) 940.

[62] B.J. Morosin, Chem. Phys. 49 (1968) 3007.

[63] J. Yang, X.-B. Wang, X.-P. Xing, L.-S. Wang, J. Chem. Phys. 128 (2008) 201102.

[64] X. Yang, X.-B. Wang, L.-S. Wang, S. Niu, T. Ichiye, J. Chem. Phys. 119 (2003), 8311.

[65] R. Cracium, D. Picone, R.T. Long, S. Li, D.A. Dixon, K.A. Peterson, K.O. Christe, Inorg. Chem. 49 (2010) 1056.

[66] R. Cracium, R.T. Long, D.A. Dixon, K.O. Christe, J. Phys. Chem. A 114 (2010) 7571

[67] A.D. Becke, J. Chem. Phys. 98 (1993) 5648.

[68] P.J. Stephens, F.J. Devlin, C.F. Chabalowski, M.J. Frisch, J. Phys. Chem. 98 (1994), 11623.

[69] Sikorska C., Smuczyn´ ska S., Skurski P., and Anusiewicz I., Inorg. Chem. 2008, 47, 7348-7354.

[70] Boldyrev A. I and Lai-Sheng Wang et al, J. Phys. Chem. A 2005, 109, 11560-11567.

[71] S. Smuczyn´ ska, P. Skurski / Chemical Physics Letters 452 (2008) 44–48.

[72] Boldyrev A I et al, J. Chem. Phys., Vol. 121, No. 12, 22 September 2004 14,15, 16, 17

[73] Boldyrev A. I and Lai-Sheng Wang et al, J. Phys. Chem. A 2005, 109, 11560-11567.

[74] Boldyrev A I et al, J. Chem. Phys., Vol. 121, No. 12, 22 September 2004.

[75] X.-B. Wang, C.-F. Ding, L.-S. Wang, A.I. Boldyrev, J. Simons,, J. Chem. Phys. 110 (1999) 4763.

[76] Boldyrev A I et al, J. Chem. Phys., Vol. 121, No. 12, 22 September 2004.

[77] X.-B. Wang, C.-F. Ding, L.-S. Wang, A.I. Boldyrev, J. Simons,, J. Chem. Phys. 110 (1999) 4763.

[78] I. Anusiewicz, P. Skurski, Chem. Phys. Lett. 358 (2002) 426.

[79] I. Anusiewicz, M. Sobczyk, I. Da˛bkowska, P. Skurski, Chem. Phys., 291 (2003) 171.

[80] Smuczynska S., Skurski P, Inorg. Chem. 2009, Vol 48, 2009.

[81] Birckenbach, L.; Kellermann, K. Ber. Dtsch. Chem. Ges. 1925, 58B, 786–794.

[82] Birckenbach, L.; Kellermann, K. Ber. Dtsch. Chem. Ges. 1925, 58B, 2377–2386.

[83] Birckenbach, L.; Huttner, K.; Stein, W. Ber. Dtsch. Chem.Ges. 1929, 62B, 2065–2075.

[84] Birckenbach, L.; Linhard, M. Ber. Dtsch. Chem. Ges. 1930, 63B, 2528–2544.

[85] Smuczynska S., Skurski P, Inorg. Chem. 2009, Vol 48, 2009.

[86] Oertel, G. Polyurethane Handbook, 3rd ed.; Hanser Publishers: Munich, 1994.

[87] Kitamura, F.; Yoshida, T. Nitto Electric Industrial Co., Ltd.: Jpn. Kokai Tokkyo Koho, JP 62,20,535 [87,20,535].

[88] Nishii, K.; Matura, A.; Takigawa, Y.; Nakada, Y. Fujitsu Ltd.: Jpn. Kokai Tokkyo Koho, JP 62,292,828 [87,292,828].

[89] Rajendran, S.; Kannan, R. Bull. Electrochem. 2000, 16, 415–418.

[90] Gutsev et al, J. Chem. Phys. 107 (10), 8 September 1997.
[91] Wang et al, J. Chem. Phys., Vol. 110, No. 10, 8 March 1999.

[92] J. Phys. Chem. A, Vol. 109, No. 50, 2005 11561.
[93] I. Anusiewicz et al. / Chemical Physics 291 (2003) 171–18015, 24.

[94] Inorganic Chemistry, Vol. 47, No. 16, 2008 7349.